JOURNAL OF COMPUTATIONAL PHYSICS **128,** 445–462 (1996)
ARTICLE NO. 0223

A Linear-Discontinuous Spatial Differencing Scheme for S_n Radiative Transfer Calculations

J. E. MOREL, TODD A. WAREING, AND KENNETH SMITH

University of California, Los Alamos National Laboratory, Los Alamos, New Mexico 87545

Received October 10, 1995; revised May 29, 1996

Various types of linear-discontinuous spatial differencing schemes have been developed for the S_n (discrete-ordinates) equations approximating the linear Boltzmann transport equation. It has been shown through an asymptotic analysis that the 1D slab-geometry lumped linear-discontinuous scheme not only goes over to a convergent and robust differencing of the diffusion equation in the monoenergetic thick diffusion limit, but it also yields the correct interior solution, even when boundary layers are left unresolved by the spatial mesh. In the present work we generalize this scheme to obtain a 1D slab-geometry lumped linear-discontinuous scheme for the nonlinear radiative transfer equation and the associated material temperature equation. We present a full nonlinear energy-dependent asymptotic analysis of the behavior of this scheme in the thick equilibrium-diffusion limit. We find that this scheme goes over to a convergent and robust differencing of the equilibrium-diffusion equation on the interior of the mesh, but it does not yield the exact interior solution when boundary layers are left unresolved by the spatial mesh. Nevertheless, the interior solution obtained with spatially unresolved boundary layers is always well behaved and fairly accurate. Computational results are presented which test the predictions of our asymptotic analysis and demonstrate the efficiency of our solution technique.

1. INTRODUCTION

Radiative transfer problems in the stellar regime are extremely challenging from a numerical point of view. Difficulties arise because the transport medium often appears optically thin to high-frequency photons, but highly optically thick to low-frequency photons. Opacities can vary over the relevant frequency range by six orders of magnitude or more. Thus it is essentially impossible to spatially resolve the intensity solution for all photon frequencies on a submean-free-path basis. In a sourceless nondiffusive region, the analytic solution is highly attenuated in optically thick cells. This means that spatial discretization schemes for the S_n equations must be able to produce *highly attenuated* solutions in such cells. Strict positivity is desirable, but not absolutely necessary. If the solution is highly attenuated and negative, it can be reset at the end of a time step to some small and positive value without significantly affecting the total radiation energy in the problem. Many simple S_n discretization schemes, such as the diamond difference scheme [1], can yield large and negative discrete solutions in optically thick cells and are thus unacceptable for radiative transfer calculations. There are other simple schemes, such as the step or upwind scheme [1], which are strictly positive. However, the step scheme can give very poor results in diffusive regions when the cells are optically thick. Counter to intuition, this can be the case even when the analytic solution varies arbitrarily slowly over a cell. The theoretical justification for this behavior arises from the fact that truncation error analysis indicates that consistent spatial discretization schemes for the S_n equations necessarily converge only in the limit as the cell width becomes small relative to a mean-free-path. A form of analysis known as a thick diffusion-limit analysis has been developed by Larsen *et. al.* [2] to provide information on the behavior of S_n spatial discretization schemes when the analytic solution is diffusive and the spatial cells are optically thick. The idea of this analysis is fairly straightforward and can be described as follows. The diffusion equation can be obtained from the transport equation by means of an asymptotic expansion. The question naturally arises as to what happens when this expansion is applied to a consistent spatially discretized form of the S_n equations. If one obtains a consistent discretization for the diffusion equation, the spatial discretization scheme is said to have the diffusion limit. In practical terms, a scheme which has the diffusion limit will yield accurate results with optically thick spatial cells as long as the variation of the analytic solution is well resolved by the mesh. However, if a scheme does not have the diffusion limit, optically thin cells are required to obtain accurate results regardless of how slowly the solution varies within each cell. These concepts are explained in a review article by Larsen on the use of asymptotic expansions for analyzing computational transport schemes [3]. Computational results presented in Ref. [2] demonstrate how startlingly inaccurate S_n schemes that do not possess the diffusion limit can be in diffusive problems with optically thick cells, even when the analytic solution hardly varies across each spatial cell. As previouly noted, it is prohibitively expensive in radiative transfer calculations to have cell widths that are optically thin for all

0021-9991/96 $18.00

photon frequencies. Thus it is essential to use S_n spatial discretization schemes that have the diffusion limit. The step or upwind scheme is strictly positive, but it does not have the thick diffusion limit and thus is generally not acceptable for radiative transfer calculations [2]. Even a scheme that has the diffusion limit can give inaccurate solutions within diffusive regions when boundary layers between transport and diffusive regions are left spatially unresolved. Although the discrete transport solution within a diffusive region satisfies a consistent discretization of the diffusion equation, failure to resolve boundary layers on the periphery of that region effectively leads to incorrect diffusion boundary conditions [2]. Although it is not impossible to resolve boundary layers in radiative transfer calculations, it is nonetheless quite difficult, and in general requires an adaptive meshing scheme. Thus it is highly desirable for S_n spatial discretization schemes used in radiative transfer calculations to give accurate solutions on the interior of diffusive regions with unresolved boundary layers. On the whole, the requirements for S_n spatial discretization schemes used in radiative transfer calculations are truly severe.

Several linear-discontinuous finite-element spatial differencing schemes have been developed for the standard linear form of the S_n equations [4]–[6]. These schemes have proven to be robust and accurate for a wide variety of neutral and charged-particle transport applications [7, 8]. Larsen and Morel have analyzed the asymptotic behavior of the 1D slab-geometry lumped linear-discontinuous difference scheme in the monoenergetic thick diffusion limit [9]. It was shown that this scheme not only goes over to a convergent and robust differencing of the diffusion equation in this limit, but it also yields the correct interior solution, even when boundary layers are left unresolved by the spatial mesh. This is a rather remarkable result which suggests that linear-discontinuous S_n spatial differencing schemes might be particularly useful for radiative transfer problems since such problems often include both transport-dominated regions and highly diffusive regions.

The purpose of this paper is to describe a nonlinear variant of the linear 1D slab-geometry linear-discontinuous S_n differencing scheme which we have developed for the radiative transfer equation and the associated material temperature equation. We also present an asymptotic analysis which predicts the behavior of this scheme in the thick equilibrium-diffusion limit. The original analysis developed by Larsen *et. al.* [2] is related to a monoenergetic linear diffusion limit. The nonlinear equilibrium diffusion limit which we consider in our analysis represents a physical limit actually encountered in radiative transfer calculations [10]. Our analysis indicates that on the interior of the mesh our linear-discontinuous scheme goes over to a convergent and robust differencing of the equilibrium-diffusion equation. However, our scheme does not necessarily yield the correct interior solution when boundary layers are left unresolved by the spatial mesh. This is somewhat disappointing in view of the performance of the linear-discontinuous scheme for the linear Boltzmann equation, but at least the solution is always well-behaved if not correct. Thus overall robustness is obtained.

The remainder of this paper is organized as follows. First we describe the radiative transfer and material temperature equations. Next we perform an asymptotic analysis of these equations to obtain the equilibrium-diffusion equation. Our discretized S_n and temperature equations are then derived, followed by a discrete asymptotic analysis to determine their behavior in the equilibrium-diffusion limit. Next we describe the technique used to solve our discrete equations. Computational results which confirm the predictions of our analysis are given next. Finally we give conclusions and recommendations for future work.

2. THE EQUATIONS OF RADIATIVE TRANSFER

The 1D slab-geometry radiative transfer equation is given by

$$\frac{1}{c}\frac{\partial \psi}{\partial t} + \mu \frac{\partial \psi}{\partial z} + \sigma_t \psi = \frac{1}{4\pi}\sigma_s \phi + \sigma_a B(T), \tag{1}$$

where c denotes the speed of light, t is the time variable, z is the spatial variable, μ is the directional variable, $\psi(t, z, \mu, \nu)$ is the angular intensity (*energy/area—time—frequency—steradian*), $\sigma_t(z, \nu)$ is the extinction coefficient (absorption plus scattering) ($length^{-1}$), $\sigma_s(z, \nu)$ is the scattering coefficient ($length^{-1}$), $\sigma_a(z, \nu)$ is the absorption coefficient ($length^{-1}$), T is the material temperature, $B(T, \nu)$ is the Planck function (*energy/area—time—frequency—steradian*), and $\phi(z, \nu)$ is the direction-integrated intensity:

$$\phi = 2\pi \int_{-1}^{+1} \psi(\mu)\, d\mu. \tag{2}$$

The Planck function is given by

$$B(T, \nu) = \frac{2h\nu^3}{c^2}\left[\exp(h\nu/kT) - 1\right]^{-1}, \tag{3}$$

where h is the Planck constant and k is the Boltzman constant. Boundary conditions for Eq. (1) can take various forms. In general, the incoming angular intensity is defined at both the left and right boundary faces. For instance, assuming the spatial domain to be the closed interval, $[z_L, z_R]$, we define the boundary conditions as

$$\psi(z_L, \mu, \nu) = f^L(\mu, \nu), \quad \mu > 0, \nu \in (0, \infty), \tag{4}$$

$$\psi(z_R, \mu, \nu) = f^B(\mu, \nu), \quad \mu < 0, \nu \in (0, \infty), \tag{5}$$

where f^L and f^R are either explicitly or implicitly specified. For instance, explicitly setting $f^L = 0$ results in a vacuum boundary condition, whereas setting $f^L(\mu, \nu) = \psi(z_L, -\mu, \nu)$ results in a reflective condition. The material temperature equation is

$$C_v \frac{\partial T}{\partial t} = \int_0^\infty \sigma_a(\phi - 4\pi B(T))\, d\nu + Q, \tag{6}$$

where C_v is the heat capacity (*energy/volume—temperature*), and Q is the material energy source (*energy/volume—time*). Equations (1) and (6) are valid under the assumption that the material is in local thermodynamic equilibrium.

3. THE EQULIBRIUM-DIFFUSION LIMIT

In this section we use an asymptotic method to derive the equilibrium-diffusion equation. This derivation is similar to that given by Larsen, *et. al.* [10]. We begin by scaling certain physical constants in Eqs. (1) and (6) with a small-parameter, ε. In particular, the following replacements are made:

$$c \to \frac{c}{\varepsilon}, \tag{7}$$

$$\sigma_t \to \frac{\sigma_t}{\varepsilon}, \tag{8}$$

$$\sigma_a \to \frac{\sigma_t}{\varepsilon} - \sigma_s, \tag{9}$$

$$C_v \to C_v \varepsilon, \tag{10}$$

$$Q \to Q\varepsilon. \tag{11}$$

These scalings can be physically interpreted as follows in the limit as $\varepsilon \to 0$: The scaling defined by Eq. (7) makes the particle speed approach infinity. The scaling defined by Eq. (8) makes the total mean-free path approach zero. The scaling defined by Eq. (9) makes the absorption mean-free-path approach zero while leaving the scattering mean-free-path unscaled. The scaling defined by Eq. (10) makes the heat capacity approach zero. The scaling defined by Eq. (11) makes the source approach zero, but this is only necessary to achieve a leading-order solution which is independent of ε. All of the other scalings are required to achieve a diffusive solution.

Substituting from Eqs. (7) through (11) into Eqs. (1) and (6), we obtain the following scaled transport and temperature equations:

$$\varepsilon^2 \frac{1}{c} \frac{\partial \psi}{\partial t} + \varepsilon\mu \frac{\partial \psi}{\partial z} + \sigma_t \psi = \frac{1}{4\pi} \varepsilon\sigma_s \phi + (\sigma_t - \varepsilon\sigma_s) B(T), \tag{12}$$

$$\varepsilon^2 C_v \frac{\partial T}{\partial t} = \int_0^\infty (\sigma_t - \varepsilon\sigma_s)(\phi - 4\pi B)\, d\nu + \varepsilon^2 Q. \tag{13}$$

Next we assume that the intensity and temperature solutions can be expanded in a power series in ε:

$$\psi = \sum_{n=0}^{\infty} \psi^{(n)} \varepsilon^n, \tag{14}$$

$$T = \sum_{n=0}^{\infty} T^{(n)} \varepsilon^n. \tag{15}$$

(16)

Since the Planck function is an explicit function of temperature, it follows that

$$B = B^{(0)} + B^{(1)}\varepsilon + B^{(2)}\varepsilon^2 + \cdots, \tag{17}$$

where

$$\begin{aligned} B^{(0)} &= B|_{\varepsilon=0}, \\ &= B|_{T=T^{(0)}}. \end{aligned} \tag{18}$$

$$\begin{aligned} B^{(1)} &= \left.\frac{\partial B}{\partial \varepsilon}\right|_{\varepsilon=0}, \\ &= \left.\frac{\partial B}{\partial T}\frac{\partial T}{\partial \varepsilon}\right|_{\varepsilon=0}, \\ &= \left.\frac{\partial B}{\partial T}\right|_{T=T^{(0)}} T^{(1)}, \quad \text{etc.} \end{aligned} \tag{19}$$

Since the heat capacity and the absorption and scattering coefficients also depend explicitly upon temperature, expansions analogous to Eq. (17) are assumed for these quantities:

$$C_v = C_v^{(0)} + C_v^{(1)}\varepsilon + C_v^{(2)}\varepsilon^2 + \cdots, \tag{20}$$

$$\sigma_s = \sigma_s^{(0)} + \sigma_s^{(1)}\varepsilon + \sigma_s^{(2)}\varepsilon^2 + \cdots, \tag{21}$$

$$\sigma_a = \sigma_a^{(0)} + \sigma_a^{(1)}\varepsilon + \sigma_a^{(2)}\varepsilon^2 + \cdots. \tag{22}$$

Substituting from Eqs. (14) through (22) into Eqs. (12) and (13), we obtain an infinite heirarchical set of equations by recognizing that each equation must independently hold

for the coefficients of like powers of ε. In particular, the equations for ε^0 are

$$\sigma_t^{(0)}\psi^{(0)} = \sigma_t^{(0)}B^{(0)} \tag{23}$$

and

$$\int_0^\infty \sigma_t^{(0)}(\phi^{(0)} - 4\pi B^{(0)})\, d\nu = 0. \tag{24}$$

Solving Eq. (23) for $\psi^{(0)}$, we obtain

$$\psi^{(0)} = B^{(0)}. \tag{25}$$

Thus we find from Eq. (25) that the zeroth order angular intensity solution is isotropic in direction and Planckian in spectral shape. Note that, since $B^{(0)} = B(T^{(0)})$, this intensity solution is completely defined by the zeroth order temperature solution. Integrating Eq. (25) over all directions, we get

$$\phi^{(0)} = 4\pi B^{(0)}, \tag{26}$$

which is consistent with Eq. (25). Integrating Eq. (26) over all frequencies, we get

$$4\pi \int_0^\infty \phi^{(0)}\, d\nu = acT^{(0)^4}, \tag{27}$$

where a is the Planck radiation constant (*energy/—volume—temperature*^{4}).

The equations for ε^1 are

$$\mu\frac{\partial\psi^{(0)}}{\partial z} + \sigma_t^{(0)}\psi^{(1)} + \sigma_t^{(1)}\psi^{(0)} = \frac{1}{4\pi}\sigma_s^{(0)}\phi^{(0)} + \sigma_t^{(0)}B^{(1)} + \sigma_t^{(1)}B^{(0)} - \sigma_s^{(0)}B^{(0)} \tag{28}$$

and

$$\int_0^\infty [\sigma_t^{(0)}(\phi^{(1)} - 4\pi B^{(1)}) + \sigma_t^{(1)}(\phi^{(0)} - 4\pi B^{(0)}) - \sigma_s^{(0)}(\phi^{(0)} - 4\pi B^{(0)})]\, d\nu = 0. \tag{29}$$

Using Eqs. (25) and (26), we simplify Eqs. (28) and (29), respectively, as

$$\mu\frac{\partial B^{(0)}}{\partial z} + \sigma_t^{(0)}\psi^{(1)} = \sigma_t^{(0)}B^{(1)} \tag{30}$$

and

$$\int_0^\infty \sigma_t^{(0)}(\phi^{(1)} - 4\pi B^{(1)})\, d\nu = 0. \tag{31}$$

Solving Eq. (30) for $\psi^{(1)}$, we obtain

$$\psi^{(1)} = -\frac{\mu}{\sigma_t^{(0)}\mathrm{b}}\frac{\partial B^{(0)}}{\partial z} + B^{(1)}. \tag{32}$$

Substituting from Eq. (19) into Eq. (32) and reexpressing the spatial derivative term in Eq. (32), we find that

$$\psi^{(1)} = -\frac{\mu}{\sigma_t^{(0)}}\frac{\partial B(T^{(0)})}{\partial T}\frac{\partial T^{(0)}}{\partial z} + \frac{\partial B(T^{(0)})}{\partial T}T^{(0)}. \tag{33}$$

It can be seen from Eq. (33) that the first-order angular intensity solution has a linearly anisotropic directional shape and a Rosseland ($\partial B/\partial T$) spectral shape.

The equations for ε^2 are

$$\frac{1}{c}\frac{\partial\psi^{(0)}}{\partial t} + \mu\frac{\partial\psi^{(1)}}{\partial z} + \sigma_t^{(0)}\psi^{(2)} + \sigma_t^{(1)}\psi^{(1)} + \sigma_t^{(2)}\psi^{(0)} = \frac{1}{4\pi}\sigma_s^{(0)}\phi^{(1)} + \sigma_s^{(1)}\phi^{(0)} + \sigma_t^{(0)}B^{(2)} + \sigma_t^{(1)}B^{(1)} + \sigma_t^{(2)}B^{(0)} - \sigma_s^{(0)}B^{(1)} - \sigma_s^{(1)}B^{(0)} \tag{34}$$

and

$$C_v^{(0)}\frac{\partial T^{(0)}}{\partial t} = \int_0^\infty [\sigma_t^{(0)}(\phi^{(2)} - 4\pi B^{(2)}) + \sigma_t^{(1)}(\phi^{(1)} - 4\pi B^{(1)}) + \sigma_t^{(2)}(\phi^{(0)} - 4\pi B^{(0)}) - \sigma_s^{(0)}(\phi^{(1)} - 4\pi B^{(1)}) - \sigma_s^{(1)}(\phi^{(0)} - 4\pi B^{(0)})]\, d\nu + Q. \tag{35}$$

Using Eqs. (25) and (26) to simplify Eqs. (34) and (35), respectively, we obtain

$$\frac{1}{c}\frac{\partial\psi^{(0)}}{\partial t} + \mu\frac{\partial\psi^{(1)}}{\partial z} + \sigma_t^{(0)}\psi^{(2)} + \sigma_t^{(1)}\psi^{(1)} = \frac{1}{4\pi}\sigma_s^{(0)}\phi^{(1)} + \sigma_t^{(0)}B^{(2)} + \sigma_t^{(1)}B^{(1)} - \sigma_s^{(0)}B^{(1)} \tag{36}$$

and

$$C_v^{(0)}\frac{\partial T^{(0)}}{\partial t} = \int_0^\infty [\sigma_t^{(0)}(\phi^{(2)} - 4\pi B^{(2)}) + (\sigma_t^{(1)} - \sigma_s^{(0)})(\phi^{(1)} - 4\pi B^{(1)})]\, d\nu + Q. \tag{37}$$

Integrating Eq. (36) over all directions and frequencies while taking Eq. (27) into account, we obtain

$$a\frac{\partial T^{(0)^4}}{\partial t} + \int_0^\infty 2\pi \int_{-1}^{+1} \mu \frac{\partial \psi^{(1)}}{\partial z}\, d\mu\, d\nu + \int_0^\infty [\sigma_t^{(0)}(\phi^{(2)} - 4\pi B^{(2)}) - (\sigma_t^{(1)} - \sigma_s^{(0)})(\phi^{(1)} - 4\pi B^{(1)})]\, d\nu = 0. \quad (38)$$

Substituting from Eq. (37) into Eq. (38), we find that

$$C_v^{(0)}\frac{\partial T^{(0)}}{\partial t} + a\frac{\partial T^{(0)^4}}{\partial t} + \int_0^\infty 2\pi \int_{-1}^{+1} \mu \frac{\partial \psi^{(1)}}{\partial z}\, d\mu\, d\nu = Q. \quad (39)$$

Reexpressing the time-derivative of $T^{(0)^4}$ in Eq. (39), we get

$$(C_v^{(0)} + 4aT^{(0)^3})\frac{\partial T^{(0)}}{\partial t} + \int_0^\infty 2\pi \int_{-1}^{+1} \mu \frac{\partial \psi^{(1)}}{\partial z}\, d\mu\, d\nu = Q. \quad (40)$$

Substituting from Eq. (33) into Eq. (40) and evaluating the integral over the angle, we obtain

$$(C_v^{(0)} + 4aT^{(0)^3})\frac{\partial T^{(0)}}{\partial t} - \int_0^\infty \frac{\partial}{\partial z}\frac{4\pi}{3\sigma_t^{(0)}}\frac{\partial B}{\partial T}\frac{\partial T^{(0)}}{\partial z}\, d\nu = Q. \quad (41)$$

Moving the frequency integral through the first spatial derivative in Eq. (41), we get

$$(C_v^{(0)} + 4aT^{(0)^3})\frac{\partial T^{(0)}}{\partial t} - \frac{\partial}{\partial z}\frac{1}{3}\left[\int_0^\infty \frac{4\pi}{\sigma_t^{(0)}}\frac{\partial B^{(0)}}{\partial T}\, d\nu\right]\frac{\partial T^{(0)}}{\partial z} = Q. \quad (42)$$

Recognizing that

$$\int_0^\infty 4\pi \frac{\partial B^{(0)}}{\partial T}\, d\nu = 4acT^{(0)^3}, \quad (43)$$

we both divide and multiply the frequency integral in Eq. (42) by the integral of $\partial B/\partial T$ to obtain the equilibrium diffusion equation in standard form,

$$(C_v^{(0)} + 4aT^{(0)^3})\frac{\partial T^{(0)}}{\partial t} - \frac{\partial}{\partial z} D^{(0)}\frac{\partial T^{(0)}}{\partial z} = Q, \quad (44)$$

where

$$D^{(0)} = \frac{4acT^{(0)^3}}{3\langle \sigma_t^{(0)}\rangle} \quad (45)$$

and

$$\frac{1}{\langle \sigma_t^{(0)}\rangle} = \frac{1}{4acT^{(0)^3}}\int_0^\infty \frac{4\pi}{\sigma_t^{(0)}}\frac{\partial B^{(0)}}{\partial T}\, d\nu. \quad (46)$$

Note from Eq. (46) that $\langle \sigma_t^{(0)}\rangle$ is the standard Rosseland-mean extinction coefficient.

Thus we see from Eqs. (25) and (44) that, to zeroth order in the asymptotic limit, the solution to the radiation transport equation goes to an isotropic and locally Planckian function of the material temperature and the material temperature satisfies a nonlinear diffusion equation.

The analysis that we have presented does not address the question of boundary conditions for Eq. (44). A boundary-layer analysis is required to address this question. However, such an analysis would be quite difficult since it essentially requires an exact solution of the transport and material temperature equations for the problem of interest, i.e., the problem for which diffusion boundary conditions are desired.

We are interested in a steady-state problem consisting of a homogeneous half-space with reflective boundary conditions at infinity,

$$\psi(\infty, \mu, \nu) = \psi(\infty, -\mu, \nu), \quad (47)$$

and an arbitrary angular intensity incident at $z = 0$,

$$\psi(0, \mu, \nu) = f(\mu, \nu) \quad \text{for } \mu > 0, \quad (48)$$

It can be shown that, at all points sufficiently deep in the interior, the temperature solution is constant, and the transport solution is constant, isotropic in angle, and Planckian in spectral shape. The equilibrium-diffusion equation will give the exact interior solution if one specifies the correct boundary conditions. The correct condition at infinity is simply that the gradient of the temperature is zero, and the correct condition at $z = 0$ is that the temperature equals the correct interior temperature, T_∞. We seek an expression for this interior temperature as a function of the incident angular intensity. To our knowledge, an exact expression has not been derived, but Pomraning [11] has derived an approximate expression using a variational technique. Specifically,

$$T_\infty^4 = T_s^4 + g(T_s), \quad (49)$$

where

$$T_s^4 = \frac{8\pi}{ac}\int_0^\infty \int_0^1 \mu f(\mu, \nu)\, d\mu\, d\nu, \tag{50}$$

$$g(T) = \frac{\langle \sigma_a \rangle}{ac}\int_0^\infty 2\pi \int_0^1 \frac{3\mu^2}{\sigma_a(\nu, T)} \times [f(\mu, \nu) - B(\nu, T)]\, d\mu\, d\nu, \tag{51}$$

$$\frac{1}{\langle \sigma_a \rangle} = \frac{\pi}{acT^3}\int_0^\infty \frac{1}{\sigma_a(\nu, T)}\frac{\partial B(\nu, T)}{\partial T}\, d\nu. \tag{52}$$

The quantity denoted by T_s is referred to as the surface temperature. Note that Pomraning's analysis does not include scattering.

4. THE DISCRETE EQUATIONS

The derivation of our discrete equations begins by assuming the standard discrete ordinates or S_n discretization [1] in the angle, the standard multigroup discretization [1] in the frequency, and the standard backward-Euler discretization in time for Eqs. (1) and (6), respectively,

$$\frac{1}{c\,\Delta t^n}(\psi_{m,g}^{n+1/2} - \psi_{m,g}^{n-1/2}) + \mu_m \frac{\partial \psi_{m,g}^{n+1/2}}{\partial z} + \sigma_{t,g}^n \psi_{m,g}^{n+1/2} = \frac{1}{4\pi}\sigma_{s,g}^n \phi_g^{n+1/2} + \sigma_a^n B_g(T^{n+1/2}), \tag{53}$$

$$\phi_g = \sum_{m=1}^{M} \psi_{m,g} w_m, \tag{54}$$

$$\frac{C_v^n}{\Delta t^n}(T^{n+1/2} - T^{n-1/2}) = \sum_{g=1}^{G} \sigma_{a,g}^n(\phi_g^{n+1/2} - 4\pi B_g(T^{n+1/2})) + Q, \tag{55}$$

where n is the time index, Δt denotes the time step, m is the direction index, M denotes the total number of discrete directions, w_m denotes the angular quadrature weight for direction m, g is the group or frequency index, and G denotes the total number of photon frequency groups. Note that quadrature is usually chosen to be Gaussian and that the weights sum to 4π. The transport coefficients (extinction, absorption, and scattering) and the heat capacity change with time because they depend upon the temperature. However, they are not evaluated at the implicit time-centered value of the temperature, i.e., $(T^{n+1/2} + T^{n-1/2})/2$, but rather at an explicit extrapolated value calculated as

$$T^n = T^{n-1/2} + \left(\frac{T^{n-1/2} - T^{n-3/2}}{t^{n-1/2} - t^{n-3/2}}\right)\frac{\Delta t^{n-1}}{2}. \tag{56}$$

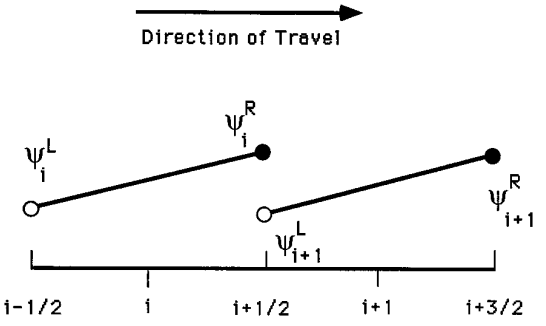

FIG. 1. Spatial dependence of angular intensity for $\mu > 0$. Note that the intensity at a cell interface is defined by the solution in the cell from which the radiation emerges.

An explicit temporal treatment of the Planck function generally results in instabilities unless extremely small time steps are taken, but we have found no difficulties with our explicit treatment of the transport coefficients. For simplicity, we henceforth suppress the time indices n and $n + 1/2$ in all the equations which follow.

The spatial discretization is begun by partitioning the spatial domain, $[z_L, z_R]$, into the usual set of contiguous cells: $(z_{i-1/2}, z_{i+1/2})$, $i = 1, N$, with $z_{1/2} = z_L$ and $z_{N+1/2} = z_R$. The material is assumed to be homogeneous within each cell, and the heat-capacity and transport coefficients within each cell are evaluated at the linear average of the left and right extrapolated cell temperatures. Next we assume a linear-discontinuous representation for the angular intensity within each cell. Specifically, the dependence on the *interior* of cell i is given by

$$\psi_{m,g}(z) = \psi_{i,m,g}^L V_i^L(z) + \psi_{i,m,g}^R V_i^R(z), \tag{57}$$

where

$$V_i^L(z) = \frac{z_{i+1/2} - z}{\Delta z_i}, \tag{58}$$

$$V_i^R(z) = \frac{z - z_{i-1/2}}{\Delta z_i}, \tag{59}$$

and

$$\Delta z_i = z_{i+1/2} - z_{i-1/2}. \tag{60}$$

The angular intensity at cell *interfaces* is defined to be continuous in the direction of radiation flow, i.e.,

$$\psi(z_{i+1/2})_{m,g} = \psi_{i,m,g}^R \quad \text{for } \mu > 0, \tag{61}$$

$$= \psi_{i+1,m,g}^L \quad \text{for } \mu < 0. \tag{62}$$

These interface intensity definitions are of fundamental importance to the linear-discontinuous scheme. Changing these definitions completely changes its behavior. The complete spatial dependence of the angular intensity is illustrated in Fig. 1 for $\mu > 0$ and in Fig. 2 for $\mu < 0$.

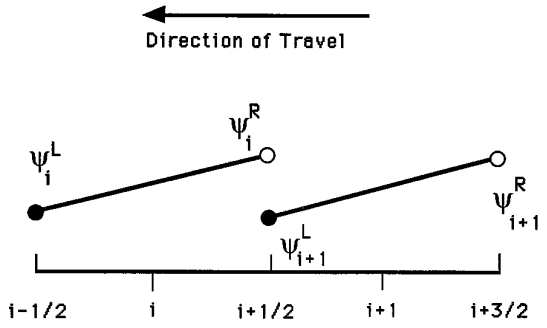

FIG. 2. Spatial dependence of angular intensity for $\mu > 0$. As in Fig. 1 the intensity at a cell interface is defined by the solution in the cell from which the radiation emerges.

We next assume a dependence for the material temperature on the *interior* of cell i that is analogous to Eq. (57). Specifically, the temperature within cell i is given by

$$T(z) = T_i^{\mathrm{L}} V_i^{\mathrm{L}}(z) + T_i^{\mathrm{R}} V_i^{\mathrm{R}}(z). \tag{63}$$

There is no need to define the material temperature at cell interfaces because our equations do not contain any spatial derivatives of the temperature. Spatial derivatives of the trial-space elements take on a delta-function dependence at the interfaces because of the element discontinuities. Thus when the finite-element integrals are performed, differential terms bring interface values into the discrete equations, whereas nondifferential terms do not.

If we were to make the usual finite-element Galerkin approximation, we would assume that the spatial dependence of the Planck function is given by $B(T(z))$, where $T(z)$ is defined according to Eq. (63). However, this assumption is fraught with numerical difficulty due to the nonlinear dependence of the Planck function on temperature. Instead we assume that the spatial dependence of the Planck function is linear-discontinuous. Specifically, the Planck function within cell i is given by Eq. (63):

$$B_g(z) = B_g(T_i^{\mathrm{L}}) V_i^{\mathrm{L}}(z) + B_g(T_i^{\mathrm{R}}) V_i^{\mathrm{R}}(z), \tag{64}$$

$$= B_{i,g}^{\mathrm{L}} V_i^{\mathrm{L}}(z) + B_{i,g}^{\mathrm{R}} V_i^{\mathrm{L}}(z). \tag{65}$$

As in the case of temperature, there is no need to define the Planck function at cell interfaces.

The spatially discretized equations are obtained as follows:

1. Substitute from Eqs. (57), (61), (62), (63), and (65), into Eqs. (53) and (55), respectively.

2. Multiply Eqs. (53) and (55), respectively, by $V_i^{\mathrm{L}}(z)$ and integrate each resulting equation over spatial cell i.

3. Multiply Eqs. (53) and (55), respectively, by $V_i^{\mathrm{R}}(z)$ and integrate each resulting equation over spatial cell i.

The equation for $\psi_{i,m,g}^{\mathrm{L}}$ with $\mu_m > 0$ is

$$\begin{aligned}
&\frac{\Delta z_i}{c\,\Delta t}\left[\left(\frac{2}{3}\psi_{i,m,g}^{\mathrm{L}} + \frac{1}{3}\psi_{i,m,g}^{\mathrm{R}}\right) - \left(\frac{2}{3}\psi_{i,m,g}^{\mathrm{L},n-1/2} + \frac{1}{3}\psi_{i,m,g}^{\mathrm{R},n+1/2}\right)\right] \\
&\quad + \mu_m[\psi_{i,m,g}^{\mathrm{L}} + \psi_{i,m,g}^{\mathrm{R}} - 2\psi_{i-1,mg}^{\mathrm{R}}] \\
&\quad + \sigma_{t,g}\,\Delta z_i\left[\frac{2}{3}\psi_{i,m,g}^{\mathrm{L}} + \frac{1}{3}\psi_{i,m,g}^{\mathrm{R}}\right] \\
&= \frac{1}{4\pi}\sigma_{s,i,g}\,\Delta z_i\left[\frac{2}{3}\phi_{i,g}^{\mathrm{L}} + \frac{1}{3}\phi_{i,g}^{\mathrm{R}}\right] \\
&\quad + \sigma_{a,i,g}\,\Delta z_i\left[\frac{2}{3}B_{i,g}^{\mathrm{L}} + \frac{1}{3}B_{i,g}^{\mathrm{R}}\right].
\end{aligned} \tag{66}$$

When i is equal to 1 (the first cell) one simply substitutes the incoming angular intensity for $\psi_{i-1,m,g}^{\mathrm{R}}$ in Eq. (66). The equation for $\psi_{i,m,g}^{\mathrm{R}}$ with $\mu_m > 0$ is

$$\begin{aligned}
&\frac{\Delta z_i}{c\,\Delta t}\left[\left(\frac{1}{3}\psi_{i,m,g}^{\mathrm{L}} + \frac{2}{3}\psi_{i,m,g}^{\mathrm{R}}\right) - \left(\frac{1}{3}\psi_{i,m,g}^{\mathrm{L},n-1/2} + \frac{2}{3}\psi_{i,m,g}^{\mathrm{R},n-1/2}\right)\right] \\
&\quad + \mu_m[\psi_{i,m,g}^{\mathrm{R}} - \psi_{i,m,g}^{\mathrm{L}}] \\
&\quad + \sigma_{t,g}\,\Delta z_i\left[\frac{1}{3}\psi_{i,m,g}^{\mathrm{L}} + \frac{1}{3}\psi_{i,m,g}^{\mathrm{R}}\right] \\
&= \frac{1}{4\pi}\sigma_{s,i,g}\,\Delta z_i\left[\frac{1}{3}\phi_{i,g}^{\mathrm{L}} + \frac{2}{3}\phi_{i,g}^{\mathrm{R}}\right] \\
&\quad + \sigma_{a,i,g}\,\Delta z_i\left[\frac{1}{3}B_{i,g}^{\mathrm{L}} + \frac{2}{3}B_{i,g}^{\mathrm{R}}\right].
\end{aligned} \tag{67}$$

The equation for $\psi_{i,m,g}^{\mathrm{L}}$ with $\mu_m < 0$ is

$$\begin{aligned}
&\frac{\Delta z_i}{c\,\Delta t}\left[\left(\frac{2}{3}\psi_{i,m,g}^{\mathrm{L}} + \frac{1}{3}\psi_{i,m,g}^{\mathrm{R}}\right) - \left(\frac{2}{3}\psi_{i,m,g}^{\mathrm{L},n-1/2} + \frac{1}{3}\psi_{i,m,g}^{\mathrm{R},n-1/2}\right)\right] \\
&\quad + \mu_m[\psi_{i,m,g}^{\mathrm{R}} - \psi_{i,m,g}^{\mathrm{L}}] \\
&\quad + \sigma_{t,g}\,\Delta z_i\left[\frac{2}{3}\psi_{i,m,g}^{\mathrm{L}} + \frac{1}{3}\psi_{i,m,g}^{\mathrm{R}}\right] \\
&= \frac{1}{4\pi}\sigma_{s,i,g}\,\Delta z_i\left[\frac{2}{3}\phi_{i,g}^{\mathrm{L}} + \frac{1}{3}\phi_{i,g}^{\mathrm{R}}\right] \\
&\quad + \sigma_{a,i,g}\,\Delta z_i\left[\frac{2}{3}B_{i,g}^{\mathrm{L}} + \frac{1}{3}B_{i,g}^{\mathrm{R}}\right].
\end{aligned} \tag{68}$$

The equation for $\psi^{R}_{i,m,g}$ with $\mu_m < 0$ is

$$\begin{aligned}
&\frac{\Delta z_i}{c\,\Delta t}\left[\left(\frac{1}{3}\,\psi^{L}_{i,m,g}+\frac{2}{3}\,\psi^{R}_{i,m,g}\right)-\left(\frac{2}{3}\,\psi^{L,n-1/2}_{i,m,g}+\frac{1}{3}\,\psi^{R,n-1/2}_{i,m,g}\right)\right]\\
&\quad+\mu_m[2\psi^{L}_{i+1,m,g}-\psi^{L}_{i,m,g}-\psi^{R}_{i,m,g}]\\
&\quad+\sigma_{t,g}\,\Delta z_i\left[\frac{1}{3}\,\psi^{L}_{i,m,g}+\frac{1}{3}\,\psi^{R}_{i,m,g}\right] \qquad (69)\\
&=\frac{1}{4\pi}\,\sigma_{s,i,g}\,\Delta z_i\left[\frac{1}{3}\,\phi^{L}_{i,g}+\frac{2}{3}\,\phi^{R}_{i,g}\right]\\
&\quad+\sigma_{a,i,g}\,\Delta z_i\left[\frac{1}{3}\,B^{L}_{i,g}+\frac{2}{3}\,B^{R}_{i,g}\right].
\end{aligned}$$

When i is equal to N (the right boundary cell) the incident angular intensity defined by the boundary condition is substituted for $\psi^{L}_{i+1,m,g}$ in Eq. (69). The equation for T^{L}_{i} is

$$\begin{aligned}
&\frac{C_{v,i}\,\Delta z_i}{\Delta t}\left[\left(\frac{2}{3}\,T^{L}_{i}+\frac{1}{3}\,T^{R}_{i}\right)-\left(\frac{2}{3}\,T^{L,n-1/2}_{i}+\frac{1}{3}\,T^{R,n-1/2}_{i}\right)\right]\\
&\quad=\sum_{g=1}^{G}\sigma_{a,i,g}\,\Delta z_i\left[\left(\frac{2}{3}\,\phi^{L}_{i,g}+\frac{1}{3}\,\phi^{R}_{i,g}\right)\right. \qquad (70)\\
&\quad\left.-4\pi\left(\frac{2}{3}\,B^{L}_{i,g}+\frac{1}{3}\,B^{R}_{i,g}\right)\right]+\left(\frac{2}{3}\,Q^{L}_{i}+\frac{1}{3}\,Q^{R}_{i}\right)\Delta z_i.
\end{aligned}$$

The equation for T^{R}_{i} is

$$\begin{aligned}
&\frac{C_{v,i}\,\Delta z_i}{\Delta t}\left[\left(\frac{1}{3}\,T^{L}_{i}+\frac{2}{3}\,T^{R}_{i}\right)-\left(\frac{1}{3}\,T^{L,n-1/2}_{i}+\frac{2}{3}\,T^{R,n-1/2}_{i}\right)\right]\\
&\quad=\sum_{g=1}^{G}\sigma_{a,i,g}\,\Delta z_i\left[\left(\frac{1}{3}\,\phi^{L}_{i,g}+\frac{2}{3}\,\phi^{R}_{i,g}\right)\right. \qquad (71)\\
&\quad\left.-4\pi\left(\frac{1}{3}\,B^{L}_{i,g}+\frac{2}{3}\,B^{R}_{i,g}\right)\right]+\left(\frac{1}{3}\,Q^{L}_{i}+\frac{2}{3}\,Q^{R}_{i}\right)\Delta z_i.
\end{aligned}$$

In order to achieve greater robustness, we ''lump'' all of the spatial averages appearing in Eqs. (66) through (71). This is a well-known technique which achieves greater robustness at the cost of accuracy. In this particular case, our spatial approximation is reduced from $O(\Delta z^3)$ accuracy [7] to $O(\Delta z^2)$ accuracy. For instance, consider the following problem:

$$\mu\frac{\partial\psi}{\partial z}+\sigma_t\psi=0,\quad z\in(0,1),\ \psi(0)=1. \qquad (72)$$

The analytic solution to this problem is

$$\psi(z)=\exp\left(-\frac{\sigma_t z}{\mu}\right), \qquad (73)$$

The linear-discontinuous solution to this equation at $z = 1$ is the Padé (1, 2) approximation to the exponential,

$$\psi(1)=\frac{1-\tau/3}{1+2\tau/3+\tau^2/6}, \qquad (74)$$

where

$$\tau=\sigma_t/\mu. \qquad (75)$$

The lumped linear-discontinuous solution to this problem at $z = 1$ is the Padé (0, 2) approximation to the exponential,

$$\psi(1)=\frac{1}{1+\tau+\tau^2/2}. \qquad (76)$$

The linear-discontinuous solution is third-order accurate in τ, but it is negative for $\tau > 3$. The lumped linear-discontinuous solution is only second-order accurate in τ, but it is strictly positive. Thus the lumped scheme is indeed less accurate but more robust.

The lumped equation for $\psi^{L}_{i,m,g}$ with $\mu_m > 0$ is

$$\begin{aligned}
&\frac{\Delta z_i}{c\,\Delta t}(\psi^{L}_{i,m,g}-\psi^{L,n-1/2}_{i,m,g})\\
&\quad+\mu_m(\psi^{L}_{i,m,g}+\psi^{R}_{i,m,g}-2\psi^{R}_{i-1,m,g})+\sigma_{t,g}\,\Delta z_i\psi^{L}_{i,m,g} \qquad (77)\\
&=\frac{1}{4\pi}\,\sigma_{s,i,g}\,\Delta z_i\phi^{L}_{i,g}+\sigma_{a,i,g}\,\Delta z_i B^{L}_{i,g}.
\end{aligned}$$

The lumped equation for $\psi^{R}_{i,m,g}$ with $\mu_m > 0$ is

$$\begin{aligned}
&\frac{\Delta z_i}{c\,\Delta t}(\psi^{R}_{i,m,g}-\psi^{R,n-1/2}_{i,m,g})\\
&\quad+\mu_m(\psi^{R}_{i,m,g}-\psi^{L}_{i,m,g})+\sigma_{t,g}\,\Delta z_i\psi^{R}_{i,m,g} \qquad (78)\\
&=\frac{1}{4\pi}\,\sigma_{s,i,g}\,\Delta z_i\phi^{R}_{i,g}+\sigma_{a,i,g}\,\Delta z_i B^{R}_{i,g}.
\end{aligned}$$

The lumped equation for $\psi^{\mathrm{L}}_{i,m,g}$ with $\mu_m < 0$ is

$$\frac{\Delta z_i}{c\,\Delta t}(\psi^{\mathrm{L}}_{i,m,g} - \psi^{\mathrm{L},n-1/2}_{i,m,g}) + \mu_m(\psi^{\mathrm{R}}_{i,m,g} - \psi^{\mathrm{L}}_{i,m,g}) + \sigma_{t,g}\,\Delta z_i \psi^{\mathrm{L}}_{i,m,g} = \frac{1}{4\pi}\,\sigma_{s,i,g}\,\Delta z_i \phi^{\mathrm{L}}_{i,g} + \sigma_{a,i,g}\,\Delta z_i B^{\mathrm{L}}_{i,g}. \tag{79}$$

The lumped equation for $\psi^{\mathrm{R}}_{i,m,g}$ with $\mu_m < 0$ is

$$\frac{\Delta z_i}{c\,\Delta t}(\psi^{\mathrm{R}}_{i,m,g} - \psi^{\mathrm{R},n-1/2}_{i,m,g}) + \mu_m(2\psi^{\mathrm{L}}_{i+1,m,g} - \psi^{\mathrm{L}}_{i,m,g} - \psi^{\mathrm{R}}_{i,m,g}) + \sigma_{t,g}\,\Delta z_i \psi^{\mathrm{R}}_{i,m,g} = \frac{1}{4\pi}\,\sigma_{s,i,g}\,\Delta z_i \phi^{\mathrm{R}}_{i,g} + \sigma_{a,i,g}\,\Delta z_i B^{\mathrm{R}}_{i,g}. \tag{80}$$

The lumped equation for T^{L}_i is

$$\frac{C_{v,i}\,\Delta z_i}{\Delta t}(T^{\mathrm{L}}_i - T^{\mathrm{L},n-1/2}_i) = \sum_{g=1}^{G} \sigma_{a,i,g}\,\Delta z_i(\phi^{\mathrm{L}}_{i,g} - 4\pi B^{\mathrm{L}}_{i,g}) + Q^{\mathrm{L}}_i\,\Delta z_i. \tag{81}$$

The lumped equation for T^{R}_i is

$$\frac{C_{v,i}\,\Delta z_i}{\Delta t}(T^{\mathrm{R}}_i - T^{\mathrm{R},n-1/2}_i) = \sum_{g=1}^{G} \sigma_{a,i,g}\,\Delta z_i(\phi^{\mathrm{R}}_{i,g} - 4\pi B^{\mathrm{R}}_{i,g}) + Q^{\mathrm{R}}_i\,\Delta z_i. \tag{82}$$

5. A DISCRETE ASYMPTOTIC ANALYSIS

In this section, we perform a discrete asymptotic analysis on the lumped LD equations. We follow essentially the same procedure as we did with the analytic asymptotic analysis. As one would expect, the overall derivation is straightforward, but rather long and tedious. Hence we give an abbreviated derivation here. Unlike the analytic case, we are able to directly determine the asymptotic behavior of our transport scheme at spatial boundaries. In particular, we derive an expression analogous to Eq. (49) for the interior temperature solution associated with the half-space problem previously discussed in Section 3.

We begin by applying the asymptotic scaling to Eqs. (77) through (82). Next we expand the intensities and temperature solutions, transport coefficients, and heat capacities in a power series in ε, as was done in the analytic case. Finally, we equate coefficients of like powers of ε to obtain the basic hierarchical asymptotic equations. These hierarchical equations are then extensively manipulated to obtain other equations and results that yield insight into the asymptotic behavior of the discrete transport solution.

We first consider the zeroth-order equations. The equations for ε^0 are

$$\sigma^{(0)}_{t,i,g}\,\Delta z_i(\psi^{\mathrm{L},(0)}_{i,m,g} - B^{\mathrm{L},(0)}_{i,g}) = 0, \tag{83}$$

$$\sigma^{(0)}_{t,i,g}\,\Delta z_i(\psi^{\mathrm{R},(0)}_{i,m,g} - B^{\mathrm{R},(0)}_{i,g}) = 0, \tag{84}$$

$$\sum_{g=1}^{G} \sigma^{(0)}_{t,i,g}\,\Delta z_i(\phi^{\mathrm{L},(0)}_{i,g} - 4\pi B^{\mathrm{L},(0)}_{i,g}) = 0, \tag{85}$$

$$\sum_{g=1}^{G} \sigma^{(0)}_{t,i,g}\,\Delta z_i(\phi^{\mathrm{R},(0)}_{i,g} - 4\pi B^{\mathrm{R},(0)}_{i,g}) = 0. \tag{86}$$

From these order ε^0 equations we find that the zeroth-order intensities are isotropic in angle and Planckian in spectral shape:

$$\psi^{\mathrm{L},(0)}_{i,m,g} = B^{\mathrm{L},(0)}_{i,g} = \frac{\phi^{\mathrm{L},(0)}_{i,g}}{4\pi}, \tag{87}$$

$$\psi^{\mathrm{R},(0)}_{i,m,g} = B^{\mathrm{R},(0)}_{i,g} = \frac{\phi^{\mathrm{R},(0)}_{i,g}}{4\pi}. \tag{88}$$

Note that Eqs. (87) and (88) are equivalent to Eqs. (25) and (26). Thus our discrete zeroth-order results are in agreement with the analytic results.

We next consider the first-order equations. The order ε^1 equation for $\psi^{\mathrm{L}}_{i,m,g}$ with $\mu_m > 0$ is

$$\begin{aligned}\mu_m\left[(\psi^{\mathrm{L},(0)}_{i,g} + \psi^{\mathrm{R},(0)}_{i,g}) - 2\begin{Bmatrix} f_{m,g}, & \text{if } i = 1 \\ B^{\mathrm{R},(0)}_{i-1,g}, & \text{if } i \neq 1 \end{Bmatrix}\right] \\ + \Delta z_i(\sigma^{(0)}_{t,i,g}\psi^{\mathrm{L},(1)}_{i,m,g} + \sigma^{(1)}_{t,i,g}\psi^{\mathrm{L},(0)}_{i,g}) \\ = \sigma^{(0)}_{s,i,g}\,\Delta z_i\left(\frac{\phi^{\mathrm{L},(0)}_{i,g}}{4\pi} - B^{\mathrm{L},(0)}_{i,g}\right) \\ + \Delta z_i(\sigma^{(0)}_{t,i,g}B^{\mathrm{L},(1)}_{i,g} + \sigma^{(1)}_{t,i,g}B^{\mathrm{L},(0)}_{i,g}),\end{aligned} \tag{89}$$

where $f_{m,g}$ denotes the incident intensity at the left boundary. The order ε^1 equation for $\psi^{\mathrm{L}}_{i,m,g}$ with $\mu_m < 0$ is

$$\begin{aligned}\mu_m(\psi^{\mathrm{R},(0)}_{i,g} - \psi^{\mathrm{L},(0)}_{i,g}) + \Delta z_i(\sigma^{(0)}_{t,i,g}\psi^{\mathrm{L},(1)}_{i,m,g} + \sigma^{(1)}_{t,i,g}\psi^{\mathrm{L},(0)}_{i,g}) \\ = \sigma^{(0)}_{s,i,g}\,\Delta z_i\left(\frac{\phi^{\mathrm{L},(0)}_{i,g}}{4\pi} - B^{\mathrm{L},(0)}_{i,g}\right) \\ = + \Delta z_i(\sigma^{(0)}_{t,i,g}B^{\mathrm{L},(1)}_{i,g} + \sigma^{(1)}_{t,i,g}B^{\mathrm{L},(0)}_{i,g}).\end{aligned} \tag{90}$$

The order ε^1 equation for $\psi^{\mathrm{R}}_{i,m,g}$ with $\mu_m > 0$ is

$$\begin{aligned}
&\mu_m(\psi^{\mathrm{R},(0)}_{i,g} - \psi^{\mathrm{L},(0)}_{i,g}) + \Delta z_i(\sigma^{(0)}_{t,i,g}\psi^{\mathrm{R},(1)}_{i,m,g} + \sigma^{(1)}_{t,i,g}\psi^{\mathrm{R},(0)}_{i,g}) \\
&\quad = \sigma^{(0)}_{s,i,g}\,\Delta z_i\left(\frac{\phi^{\mathrm{R},(0)}_{i,g}}{4\pi} - B^{\mathrm{R},(0)}_{i,g}\right) \\
&\qquad + \Delta z_i(\sigma^{(0)}_{t,i,g}B^{\mathrm{R},(1)}_{i,g} + \sigma^{(1)}_{t,i,g}B^{\mathrm{R},(0)}_{i,g}),
\end{aligned} \tag{91}$$

and the order ε^1 equation for $\psi^{\mathrm{R}}_{i,m,g}$ with $\mu_m < 0$ is

$$\begin{aligned}
&\mu_m[-(\psi^{\mathrm{L},(0)}_{i,g} + \psi^{\mathrm{R},(0)}_{i,g}) + 2\psi^{\mathrm{L},(0)}_{i+1,g}] \\
&\qquad + \Delta z_i(\sigma^{(0)}_{t,i,g}\psi^{\mathrm{R},(1)}_{i,m,g} + \sigma^{(1)}_{t,i,g}\psi^{\mathrm{R},(0)}_{i,g}) \\
&\quad = \sigma^{(0)}_{s,i,g}\,\Delta z_i\left(\frac{\phi^{\mathrm{R},(0)}_{i,g}}{4\pi} - B^{\mathrm{R},(0)}_{i,g}\right) \\
&\qquad + \Delta z_i(\sigma^{(0)}_{t,i,g}B^{\mathrm{R},(1)}_{i,g} + \sigma^{(1)}_{t,i,g}B^{\mathrm{R},(0)}_{i,g}).
\end{aligned} \tag{92}$$

The remaining order ε^1 equations are

$$\begin{aligned}
&\sum_{g=1}^{G}\Delta z_i\{\sigma^{(0)}_{t,i,g}(\phi^{\mathrm{L},(1)}_{i,g} - 4\pi B^{\mathrm{L},(1)}_{i,g}) \\
&\qquad + (\sigma^{(1)}_{t,i,g} - \sigma^{(0)}_{s,i,g})(\phi^{\mathrm{L},(0)}_{i,g} - 4\pi B^{\mathrm{L},(0)}_{i,g})\} = 0,
\end{aligned} \tag{93}$$

$$\begin{aligned}
&\sum_{g=1}^{G}\Delta z_i\{\sigma^{(0)}_{t,i,g}(\phi^{\mathrm{R},(1)}_{i,g} - 4\pi B^{\mathrm{R},(1)}_{i,g}) \\
&\qquad + (\sigma^{(1)}_{t,i,g} - \sigma^{(0)}_{s,i,g})(\phi^{\mathrm{R},(0)}_{i,g} - 4\pi B^{\mathrm{R},(0)}_{i,g})\} = 0.
\end{aligned} \tag{94}$$

Using these first-order equations, together with the zeroth-order equations, we obtain several results. For instance, we find that the first-order angular flux is in pointwise agreement with the analytic first-order angular flux given by Eq. (32). For example, we find that for $\mu_m < 0$,

$$\psi^{\mathrm{L},(1)}_{i,m,g} = \frac{\mu_m}{\sigma^{(0)}_{t,i,g}\Delta z_i}(B^{\mathrm{R},(0)}_{i,g} - B^{\mathrm{L},(0)}_{i,g}) + B^{\mathrm{L},(1)}_{i,g}. \tag{95}$$

We find that the zeroth order intensities and temperatures are *continuous* at all but the first cell interface:

$$\sum_{g=1}^{G}B^{\mathrm{R},(0)}_{i-1,g} = \sum_{g=1}^{G}B^{\mathrm{L},(0)}_{i,g} \equiv \sum_{g=1}^{G}B^{(0)}_{i-1/2,g}, \quad i \neq 1. \tag{96}$$

We find that the temperature on the left side of the first cell is equal to the surface temperature defined by Eq. (50),

$$T^{\mathrm{L},(0)4}_{1} = \frac{2}{ac\langle\mu\rangle}\sum_{g=1}^{G}\sum_{\mu_m>0}\mu_m f_{m,g}w_m, \tag{97}$$

where

$$\langle\mu\rangle = \frac{1}{2\pi}\sum_{\mu_m>0}\mu_m w_m. \tag{98}$$

We obtain an expression for the first-order net flux on the left side of the first cell:

$$\begin{aligned}
&\sum_{g=1}^{G}\sum_{\mu_m=1}^{N}\mu_m\psi^{\mathrm{L},(1)}_{i,m,g}w_m \\
&\quad = -\frac{1}{3\,\Delta z_i}\sum_{g=1}^{G}\frac{1}{\sigma^{(0)}_{t,i,g}} \\
&\qquad \times\left(4\pi B^{\mathrm{R},(0)}_{i,g} - 2\sum_{\mu_m>0}3\mu_m^2 f_{m,g}w_m\right), \quad i = 1.
\end{aligned} \tag{99}$$

We obtain an expression for the first-order net flux on the left side of all interior cells:

$$\begin{aligned}
&\sum_{g=1}^{G}\sum_{\mu_m=1}^{N}\mu_m\psi^{\mathrm{L},(1)}_{i,m,g}w_m \\
&\quad = -\frac{1}{3\,\Delta z_i}\sum_{g=1}^{G}\frac{4\pi}{\sigma^{(0)}_{t,i,g}}(B^{\mathrm{R},(0)}_{i,g} - B^{\mathrm{L},(0)}_{i,g}), \quad i \neq 1.
\end{aligned} \tag{100}$$

Finally, we obtain an expression for the first-order net flux on the right side of all cells:

$$\begin{aligned}
&\sum_{g=1}^{G}\sum_{\mu_m=1}^{N}\mu_m\psi^{\mathrm{R},(1)}_{i,m,g}w_m \\
&\quad = -\frac{1}{3\,\Delta z_i}\sum_{g=1}^{G}\frac{4\pi}{\sigma^{(0)}_{t,i,g}}(B^{\mathrm{R},(0)}_{i,g} - B^{\mathrm{L},(0)}_{i,g}).
\end{aligned} \tag{101}$$

We next consider the second-order equations. The order ε^2 equation for $\psi^{\mathrm{L}}_{i,m,g}$ with $\mu_m > 0$ is

$$\begin{aligned}
&\frac{\Delta z_i}{c\,\Delta t}(\psi^{\mathrm{L},(0)}_{i,m,g} - \psi^{\mathrm{L},(0),n-1/2}_{i,m,g}) \\
&\qquad + \mu_m\left[(\psi^{\mathrm{L},(0)}_{i,m,g} + \psi^{\mathrm{R},(1)}_{i,m,g}) - 2\begin{Bmatrix} 0 & \text{if } i = 1 \\ \psi^{\mathrm{R},(1)}_{i-1,m,g}, & \text{if } i \neq 1 \end{Bmatrix}\right] \\
&\qquad + \Delta z_i(\sigma^{(0)}_{t,i,g}\psi^{\mathrm{L},(2)}_{i,m,g} + \sigma^{(1)}_{t,i,g}\psi^{\mathrm{L},(1)}_{i,m,g} + \sigma^{(2)}_{t,i,g}\psi^{\mathrm{L},(0)}_{i,g}) \\
&\quad = \Delta z_i\left[\sigma^{(0)}_{s,i,g}\left(\frac{\phi^{\mathrm{L},(1)}_{i,g}}{4\pi} - B^{\mathrm{L},(1)}_{i,g}\right) + \sigma^{(1)}_{s,i,g}\left(\frac{\phi^{\mathrm{L},(0)}_{i,g}}{4\pi} - B^{\mathrm{L},(0)}_{i,g}\right)\right] \\
&\qquad + \Delta z_i(\sigma^{(0)}_{t,i,g}B^{\mathrm{L},(2)}_{i,g} + \sigma^{(1)}_{t,i,g}B^{\mathrm{L},(1)}_{i,g} + \sigma^{(2)}_{t,i,g}B^{\mathrm{L},(0)}_{i,g}).
\end{aligned} \tag{102}$$

The order ε^2 equation for $\psi^{\mathrm{L}}_{i,m,g}$ with $\mu_m < 0$ is

$$\begin{aligned}
&\frac{\Delta z_i}{c\,\Delta t}(\psi^{\mathrm{L},(0)}_{i,g} - \psi^{\mathrm{L},(0),n-1/2}_{i,g}) + \mu_m(\psi^{\mathrm{R},(1)}_{i,m,g} - \psi^{\mathrm{L},(0)}_{i,m,g}) \\
&\quad + \Delta z_i(\sigma^{(0)}_{t,i,g}\psi^{\mathrm{L},(2)}_{i,m,g} + \sigma^{(1)}_{t,i,g}\psi^{\mathrm{L},(1)}_{i,m,g} + \sigma^{(2)}_{t,i,g}\psi^{\mathrm{L},(0)}_{i,g}) \\
&= \Delta z_i\left[\sigma^{(0)}_{s,i,g}\left(\frac{\phi^{\mathrm{L},(1)}_{i,g}}{4\pi} - B^{\mathrm{L},(1)}_{i,g}\right) + \sigma^{(1)}_{s,i,g}\left(\frac{\phi^{\mathrm{L},(0)}_{i,g}}{4\pi} - B^{\mathrm{L},(0)}_{i,g}\right)\right] \\
&\quad + \Delta z_i(\sigma^{(0)}_{t,i,g}B^{\mathrm{L},(2)}_{i,g} + \sigma^{(1)}_{t,i,g}B^{\mathrm{L},(1)}_{i,g} + \sigma^{(2)}_{t,i,g}B^{\mathrm{L},(0)}_{i,g}). \qquad (103)
\end{aligned}$$

The order ε^2 equation for $\psi^{\mathrm{R}}_{i,m,g}$ with $\mu_m > 0$ is

$$\begin{aligned}
&\frac{\Delta z_i}{c\,\Delta t}(\psi^{\mathrm{R},(0)}_{i,g} - \psi^{\mathrm{R},(0),n-1/2}_{i,g}) + \mu_m(\psi^{\mathrm{R},(1)}_{i,m,g} - \psi^{\mathrm{L},(1)}_{i,m,g}) \\
&\quad + \Delta z_i(\sigma^{(0)}_{t,i,g}\psi^{\mathrm{R},(2)}_{i,m,g} + \sigma^{(1)}_{t,i,g}\psi^{\mathrm{R},(1)}_{i,m,g} + \sigma^{(2)}_{t,i,g}\psi^{\mathrm{R},(0)}_{i,g}) \\
&= \Delta z_i\left[\sigma^{(0)}_{s,i,g}\left(\frac{\phi^{\mathrm{R},(1)}_{i,g}}{4\pi} - B^{\mathrm{R},(1)}_{i,g}\right) + \sigma^{(1)}_{s,i,g}\left(\frac{\phi^{\mathrm{R},(0)}_{i,g}}{4\pi} - B^{\mathrm{R},(0)}_{i,g}\right)\right] \\
&\quad + \Delta z_i(\sigma^{(0)}_{t,i,g}B^{\mathrm{R},(2)}_{i,g} + \sigma^{(1)}_{t,i,g}B^{\mathrm{R},(1)}_{i,g} + \sigma^{(2)}_{t,i,g}B^{\mathrm{R},(0)}_{i,g}). \qquad (104)
\end{aligned}$$

The order ε^2 equation for $\psi^{\mathrm{R}}_{i,m,g}$ with $\mu_m > 0$ is

$$\begin{aligned}
&\frac{\Delta z_i}{c\,\Delta t}(\psi^{\mathrm{R},(0)}_{i,m,g} - \psi^{\mathrm{R},(0),n-1/2}_{i,m,g}) + \mu_m[-(\psi^{\mathrm{L},(1)}_{i,m,g} + \psi^{\mathrm{R},(1)}_{i,m,g}) + 2\psi^{\mathrm{L},(1)}_{i+1,m,g}] \\
&\quad + \Delta z_i(\sigma^{(0)}_{t,i,g}\psi^{\mathrm{R},(2)}_{i,m,g} + \sigma^{(1)}_{t,i,g}\psi^{\mathrm{R},(1)}_{i,m,g} + \sigma^{(2)}_{t,i,g}\psi^{\mathrm{R},(0)}_{i,g}) \\
&= \Delta z_i\left[\sigma^{(0)}_{s,i,g}\left(\frac{\psi^{\mathrm{R},(1)}_{i,g}}{4\pi} - B^{\mathrm{R},(1)}_{i,g}\right) + \sigma^{(1)}_{s,i,g}\left(\frac{\phi^{\mathrm{R},(0)}_{i,g}}{4\pi} - B^{\mathrm{R},(0)}_{i,g}\right)\right] \\
&\quad + \Delta z_i(\sigma^{(0)}_{t,i,g}B^{\mathrm{R},(2)}_{i,g} + \sigma^{(1)}_{t,i,g}B^{\mathrm{R},(1)}_{i,g} + \sigma^{(2)}_{t,i,g}B^{\mathrm{R},(0)}_{i,g}). \qquad (105)
\end{aligned}$$

The remaining order ε^2 equations are

$$\begin{aligned}
&\frac{C^{(0)}_{v,i}\,\Delta z_i}{\Delta t}(T^{\mathrm{L},(0)}_i - T^{\mathrm{L},(0),n-1/2}_i) \\
&\quad = \sum_{g=1}^{G}\Delta z_i\{\sigma^{(0)}_{t,i,g}(\phi^{\mathrm{L},(2)}_{i,g} - 4\pi B^{\mathrm{L},(2)}_{i,g}) \qquad (106) \\
&\qquad + (\sigma^{(1)}_{t,i,g} - \sigma^{(0)}_{s,i,g})(\phi^{\mathrm{L},(1)}_{i,g} - 4\pi B^{\mathrm{L},(1)}_{i,g}) \\
&\qquad + [\sigma^{(2)}_{t,i,g} - \sigma^{(1)}_{s,i,g}](\phi^{\mathrm{L},(0)}_{i,g} - 4\pi B^{\mathrm{L},(0)}_{i,g})\} + Q^L_i\,\Delta z_i
\end{aligned}$$

and

$$\begin{aligned}
&\frac{C^{(0)}_{v,i}\,\Delta z_i}{\Delta t}(T^{\mathrm{R},(0)}_i - T^{\mathrm{R},(0),n-1/2}_i) \\
&\quad = \sum_{g=1}^{G}\Delta z_i\{\sigma^{(0)}_{t,i,g}(\phi^{\mathrm{R},(2)}_{i,g} - 4\pi B^{\mathrm{R},(2)}_{i,g}) \qquad (107) \\
&\qquad + [\sigma^{(1)}_{t,i,g} - \sigma^{(0)}_{s,i,\mathrm{g}}](\phi^{\mathrm{R},(1)}_{i,g} - 4\pi B^{\mathrm{R},(1)}_{i,g}) \\
&\qquad + (\sigma^{(2)}_{t,i,g} - \sigma^{(1)}_{s,i,g})(\phi^{\mathrm{R},(0)}_{t,g} - 4\pi B^{\mathrm{R},(0)}_{i,g})\} + Q^R_i\,\Delta z_i.
\end{aligned}$$

Using these second-order equations, together with the first-order equations and the zeroth-order equations, we obtain the following discrete diffusion equation on the mesh interior,

$$\begin{aligned}
&\left(C^{(0)}_{v,i+1}\frac{\Delta z_{i+1}}{2} + C^{(0)}_{v,i}\frac{\Delta z_i}{2} + 4a\tilde{T}^{(0)^3}_{i+1/2}\right)\left(\frac{T^{(0)}_{i+1/2} - T^{(0),n-1/2}_{i+1/2}}{\Delta t}\right) \\
&\quad - \frac{D^{(0)}_{i+1}}{\Delta z_{z+1}}(T^{(0)}_{i+3/2} - T^{(0)}_{i+1/2}) - \frac{D^{(0)}_i}{\Delta z_i}(T^{(0)}_{i+1/2} - T^{(0)}_{i-1/2}) \\
&\quad = Q^{\mathrm{L}}_{i+1}\frac{\Delta z_{i+1}}{2} + Q^{\mathrm{R}}_i\frac{\Delta z_i}{2}, \qquad (108)
\end{aligned}$$

where

$$4\tilde{T}^{(0)}_{i+1/2} = \left[\frac{T^{(0)^4}_{i+1/2} - T^{(0),n-1/2^4}_{i+1/2}}{T^{(0)}_{i+1/2} - T^{(0),n-1/2}_{i+1/2}}\right], \qquad (109)$$

$$D^{(0)}_i = \frac{ac4\tilde{T}^{(0)^3}_i}{3\langle\sigma^{(0)}_{t,i}\rangle}, \qquad (110)$$

$$\frac{1}{\langle\sigma^{(0)}_{i,i}\rangle} = \frac{\sum_{g=1}^{G}\frac{1}{\sigma^{(0)}_{t,i,g}}(B^{(0)}_{i+1/2,g} - B^{(0)}_{i-1/2,g})}{\sum_{g=1}^{G}(B^{(0)}_{i+1/2,g} - B^{(0)}_{i-1/2,g})}, \qquad (111)$$

$$4\tilde{T}^{(0)^3}_i = \frac{T^{(0)^4}_{i+1/2} - T^{(0)^4}_{i-1/2}}{T^{(0)}_{i+1/2} - T^{(0)}_{i-1/2}}. \qquad (112)$$

Equation (108) represents a valid discretization of the analytic equilibrium diffusion equation given by Eq. (44). Equation (108) is a three-point vertex-centered diffusion difference equation with a fully implicit one-point time-derivative term. This is a particularly robust structure for the equation. Vertex unknowns are consistent with the continuity of the zeroth-order intensities and temperatures at the interior cell interfaces. In fact, if one were to ignore the nonlinearities, this equation would be analogous to a lumped linear-*continuous* differencing of the diffusion equation. Thus it appears that our lumped linear-*discontinuous* approximation for the transport equation gives rise

to a lumped linear-*continuous* approximation for the equilibrium diffusion equation in the thick diffusion limit. Note that

$$\frac{\sum_{g=1}^{G} \frac{1}{\sigma_{t,i,g}^{(0)}} (B_{i+1/2,g}^{(0)} - B_{i-1/2,g}^{(0)})}{\sum_{g=1}^{G} (B_{i+1/2,g}^{(0)} - B_{i-1/2,g}^{(0)})} \approx \frac{\sum_{g=1}^{G} \frac{1}{\sigma_{t,i,g}^{(0)}} \frac{\partial B_{i,g}^{(0)}}{\partial T}}{\sum_{g=1}^{G} \frac{\partial B_{i,g}^{(0)}}{\partial T}}. \quad (113)$$

Thus $\langle \sigma_{t,i}^{(0)} \rangle$ represents a numerical approximation to the Rosseland extinction coefficient for cell i. Although the expressions for $\tilde{T}_{i+1/2}^{(0)}$ and $\langle \sigma_{t,i}^{(0)} \rangle$ become indeterminate (i.e., of the form 0/0) when the temperature is constant within a cell, they are nonetheless well-defined in the limit as a constant temperature is approached. It is possible to manipulate Eq. (108) to eliminate all indeterminate expressions, but the resulting equation is more difficult to recognize as an approximation to the analytic equilibrium diffusion equation. Since we do not actually solve Eq. (108) and, since the indeterminate expressions are actually well-defined, their presence is of no consequence.

As previously, noted, the temperature on the left side of the first cell assumes the surface temperature defined by Eq. (97) (a quadrature approximation to Eq. (50)). This would seem to indicate that the discrete interior solution for the model half-space problem is given by the surface temperature. However, further analysis of the asymptotic equations shows that for the model problem, the temperatures at *all points other than the first* are constant and assume the value,

$$\tilde{T}_{\infty}^4 = \tilde{T}_s^4 + \frac{1}{ac} [\sigma_{t,1}^{(0)}] \sum_{g=1}^{G} \sum_{\mu_m > 0} \frac{3\mu_m^2 [f_{m,g} - B_g(T_s)] w_m}{\sigma_{t,1,g}^{(0)}}, \quad (114)$$

where $\tilde{T}_s$ is the surface temperature calculated with the S_n angular quadrature,

$$\tilde{T}_s^4 = \frac{2}{ac\langle \mu \rangle} \sum_{g=1}^{G} \sum_{\mu_m > 0} \mu_m f_{m,g} w_m \quad (115)$$

and

$$\frac{1}{[\sigma_{t,1}^{(0)}]} = \frac{\sum_{g=1}^{G} \frac{1}{\sigma_{t,1,g}^{(0)}} [B_g(T_\infty) - B_g(T_s)]}{\sum_{g=1}^{G} [B_g(T_\infty) - B_g(T_s)]}. \quad (116)$$

Equation (114) is strikingly similar to Pomraning's variational expression for T_∞ as given by Eq. (49). This is clearly an extraordinary result that gives us confidence in the accuracy and robustness of our linear-discontinuous discretization scheme. Although Eq. (114) is similar to Eq. (49), it is not identical. There are four differences between these two expressions. First, Eq. (114) includes scattering whereas Eq. (49) does not. Second, the expression for $[\sigma_{t,1}^{(0)}]$ appearing in Eq. (114) represents a numerical approximation to the Rosseland-mean extinction coefficient appearing in Eq. (49). Third, the quantity $\sigma_{t,1,g}^{(0)}$ appearing in Eq. (114) is evaluated at the average of $\tilde{T}_s$ and $\tilde{T}_\infty$ (the average temperature in the first cell), whereas the quantity $\langle \sigma_a \rangle$ appearing in Eq. (49) is evaluated at T_s. Fourth, because $[\sigma_{t,1}^{(0)}]$ and $\sigma_{t,1,g}^{(0)}$ are explicitly dependent upon T_∞, Eq. (110) represents an implicit expression for $\tilde{T}_\infty$, whereas Eq. (49) represents an explicit expression for T_∞. Considering the numerical significance of these differences, it seems likely that $\tilde{T}_\infty$ will nearly equal T_∞ in problems without scattering. The results later given in the computational section support this conjecture.

6. SOLUTION OF THE EQUATIONS

Our solution technique is based upon the following three fundamental elements:

1. A linearization of the Planckian temperature dependence which enables the material temperature to be eliminated from the transport equation. Solution of the resulting linear transport equation represents a single Newton iteration on the non-linear system.

2. Use of the standard source iteration technique to solve the transport equation.

3. Diffusion-synthetic acceleration of the scattering source iterations. This technique is well known within the neutron transport community [12].

4. Linear multifrequency-grey acceleration of the linearized Planckian source iterations [14].

For simplicity, we initially describe our solution technique in terms of the time and energy discretized but spatially continuous equations. The linearization process begins by assuming that

$$B^{n+1/2} = B^{n-1/2} + \frac{\partial B^{n-1/2}}{\partial T} (T^{n+1/2} - T^{n-1/2}). \quad (117)$$

Substituting from Eq. (117) into Eqs. (53) and (55), we obtain, after tedious but straightforward algebraic manipulation,

$$\mu_m \frac{\partial \psi_{m,g}}{\partial z} + \hat{\sigma}_{t,g} \psi_{m,g} = \frac{1}{4\pi} \sigma_{s,g} \phi_g + \frac{1}{4\pi} \nu \chi_g \sum_{k=1}^{G} \sigma_{a,k} \phi_k + q_g + \frac{1}{c\,\Delta t} \psi_{m,g}^{n-1/2}, \quad (118)$$

$$T = \left[\sum_{g=1}^{G} \sigma_{a,g}(\phi_g - 4\pi B_g^{n-1/2}) + Q\right] \Bigg/ \left[\frac{C_v}{\Delta t} + 4\pi \sum_{g=1}^{G} \frac{\partial B_g^{n-1/2}}{\partial T}\right] + T^{n-1/2}, \tag{119}$$

where

$$\hat{\sigma}_{t,g} = \sigma_{t,g} + \frac{1}{c\,\Delta t}, \tag{120}$$

$$\nu = \left[4\pi \sum_{g=1}^{G} \sigma_{a,g} \frac{\partial B_g^{n-1/2}}{\partial T}\right] \Bigg/ \left[\frac{C_v}{\Delta t} + 4\pi \sum_{g=1}^{G} \sigma_{a,g} \frac{\partial B_g^{n-1/2}}{\partial z}\right], \tag{121}$$

$$\chi_g = \left[\sigma_{a,g} \frac{\partial B_g^{n-1/2}}{\partial T}\right] \Bigg/ \left[\sum_{g=1}^{G} \sigma_{a,k} \frac{\partial B_k^{n-1/2}}{\partial T}\right], \tag{122}$$

$$q_g = \sigma_{a,g} B_g^{n-1/2} + \frac{1}{4\pi} \nu \chi_g \left[Q - 4\pi \sum_{k=1}^{G} \sigma_{a,k} \frac{\partial B_k^{n-1/2}}{\partial T}\right]. \tag{123}$$

Note that Eq. (118) no longer depends upon the material temperature, but Eq. (119) still contains the photon intensities. Thus Eq. (118) is solved first, after which Eq. (119) is used to calculate the material temperatures. Further note from the right side of Eq. (118) that the temperature elimination process results in a coupling between the energy groups through an effective emission source. Interestingly, this emission source is mathematically equivalent to a neutron fission source with ν playing the role of the number of neutrons emitted per fission and $\{\chi_g\}_g^G$ playing the role of the fission spectrum.

Equation (118) is solved via source iteration. Specifically, the scattering and emission sources are lagged, resulting in the iteration equations

$$\mu_m \frac{\partial \psi_{m,g}^{l+1/2}}{\partial z} + \hat{\sigma}_{t,g} \psi_{m,g}^{l+1/3} = \frac{1}{4\pi} \sigma_{s,g} \phi_g^l + \frac{1}{4\pi} \nu \chi_g \sum_{k=1}^{G} \sigma_{a,k} \phi_k^l + q_g + \frac{1}{c\,\Delta t} \psi_{m,g}^{n-1/2}, \tag{124}$$

where l is the iteration index. Note that $l + \frac{1}{3}$ is used rather than $l + 1$, in anticipation of two additional acceleration steps. The left side of Eq. (124) represents a first-order ordinary differential equation for each discrete direction and energy group. When this equation is spatially differenced, a block lower-triangular matrix is obtained. The corresponding system of equations can be directly solved via a sequential set of 2×2 matrix solutions. For instance, let us assume source or vacuum conditions at both left and right boundaries. Then the incident angular intensities are known for $\mu > 0$ at the left boundary and for $\mu < 0$ at the right boundary. For a given direction and energy group with $\mu > 0$, the incident intensity at the left boundary provides the initial condition needed to solve for the two corresponding intensities in the first (leftmost) spatial cell. Solving for the intensities in the first cell provides the initial condition for the intensities in the second cell. The intensities in the second cell are then calculated and the process is continued until the intensities in the last (rightmost) cell are obtained. The solution for the intensites with $\mu < 0$ begins at the right boundary and proceeds analogously. For obvious reasons, this solution process is often referred to as a sweep.

Unfortunately, this straightforward iteration process can be very slowly convergent if either of the following conditions are met:

1. The ratio of the scattering coefficient to the extinction coefficient is near unity, i.e., $\sigma_{s,g}/\sigma_{t,g} \approx 1$.
2. The material and radiation are strongly coupled, i.e., the system is optically thick and $\nu \approx 1$.

We eliminate this poor convergence by sequentially applying two diffusion-based acceleration techniques: diffusion-synthetic acceleration [12] and linear multifrequency-grey acceleration [14]. Once a sweep has been performed for all of the directions in an energy group, a diffusion-synthetic acceleration step is performed for that group. This step begins solving the diffusion equation,

$$-\frac{\partial}{\partial z} \hat{D}_g \frac{\partial \delta\phi_g}{\partial z} + \sigma_a \delta\phi_g = \sigma_{s,g}(\phi_g^{l+1/3} - \phi_g^l), \tag{125}$$

where

$$\hat{D}_g = 1/3\hat{\sigma}_{t,g} \tag{126}$$

and where $\delta\phi_g$ denotes an estimate of the additive error in the angle-integrated intensity for group g due to the lagged scattering source. The error estimate is then added to the solution iterate at step $l + \frac{1}{3}$ under the assumption that the error has a diffusive (P_1) angular dependence. This yields the "accelerated" iterate at step $l + \frac{2}{3}$,

$$\psi_{m,g}^{l+2/3} = \psi_{m,g}^{l+1/3} + \frac{1}{4\pi} \delta\phi_g - \frac{3\mu_m}{4\pi} \hat{D}_g \nabla\, \delta\phi_g, \tag{127}$$

where $-\hat{D}_g \nabla\, \delta\phi_g$ denotes an estimate of the flux error consistent with the diffusion approximation for $\delta\phi_g$. After a sweep has been performed for each direction in each group, and a diffusion-synthetic acceleration step has been performed for each group, the linear multifrequency-grey acceleration step is performed. This step begins by solving the diffusion equation,

$$-\frac{\partial}{\partial z}\langle D\rangle\frac{\partial\delta\Phi}{\partial z}+\langle\sigma\rangle\,\delta\Phi=\nu\sum_{g=1}^{G}\sigma_{s,g}(\phi_g^{l+2/3}-\phi_g^{l}),\quad(128)$$

where

$$\langle D\rangle=\frac{1}{3}\sum_{g=1}^{G}\frac{\xi_g}{\hat{\sigma}_{t,g}},\quad(129)$$

$$\langle\sigma\rangle=\frac{1}{c\,\Delta t}+(1-\nu)\sum_{g=1}^{G}\sigma_{a,g}\xi_g,\quad(130)$$

$$\xi_g=\frac{\chi_g}{\sigma_{a,g}+1/(c\,\Delta t)}\Bigg/\sum_{k=1}^{G}\frac{\chi_k}{\sigma_{a,k}+1/(c\,\Delta t)},\quad(131)$$

and where $\delta\Phi$ denotes an estimate of the additive error in the frequency-angle-integrated intensity iterate due to the lagged emission source. Note that $\{\xi_g\}_{g=1}^{G}$ represents the assumed frequency shape of the additive error. The error estimate is then added to the solution iterate at step $l+\frac{2}{3}$ under the assumption that the error has a diffusive (P_1) angular dependence. This yields the "accelerated" iterate at step $l+1$,

$$\psi_{m,g}^{l+1}=\psi_{m,g}^{l+2/3}+\frac{1}{4\pi}\,\delta\Phi\xi_g-\frac{3\mu_m}{4\pi}\hat{D}_g\xi_g\nabla\,\delta\Phi,\quad(132)$$

where $-\hat{D}_g\xi_g\nabla\,\delta\Phi$ denotes an estimate of the flux error consistent with the diffusion approximation for $\delta\Phi$. This completes one accelerated iteration. To summarize the process, a sweep is performed for each direction in each group. A diffusion-synthetic acceleration step is then performed for each group. Finally, a single linear multifrequency-grey step is performed. Both of our acceleration schemes are very effective. Most importantly, they bound the spectral radius for the iterative process away from unity. This is later demonstrated computationally.

The general idea behind both acceleration schemes is simply to replace an exact transport equation for the iterative errors with a diffusion approximation. Because diffusion theory can be thought of as a "coarse-grid" approximation in angle to transport theory, these schemes can be interpreted as two-grid multigrid schemes. These schemes are effective because the transport sweep strongly attenuates all error modes other than those which are diffusive. In the case of diffusion-synthetic acceleration, the diffusive modes are those which are nearly isotropic in angle. In the case of linear multifrequency-grey acceleration, the diffusive modes are those which are both nearly isotropic in angle and fixed in frequency shape. These points are discussed in detail in Refs. [12, 15]. Note that, although a fission-source acceleration scheme is described in Ref. [15], it is nonetheless directly applicable to our problem because our linearized equations are mathematically equivalent to the neutron transport equation with fission. In principle, the boundary conditions for the acceleration equations are chosen so that the accelerated iterates (Eq. (127) in the case of diffusion-synthetic acceleration and Eq. (132) in the case of linear multifrequency-grey acceleration) satisfy the correct boundary conditions. However, since the boundary conditions cannot always be exactly satisfied, they are often satisfied in an integral sense. This principle is discussed in Ref. [16]. The boundary conditions that we use ensure that the accelerated iterate at step $l+1$ satisfies both local and global energy conservation. This is a highly desirable property since it enables us to terminate the iteration process sooner than otherwise would be possible.

As previously noted, the solution of the linearized equations represents a single Newton iteration on the full system. While it is possible to continue the Newton iterations and obtain a fully converged nonlinear solution, we generally do not do so. We have found that a single Newton iteration is provides temporal stability and adequate accuracy for our purposes. However, our discrete asymptotic analysis rigorously applies only if the Newton iterations are continued to convergence.

We now give the discrete linearized equations. The linearized lumped equation for $\psi_{i,m,g}^{\mathrm{L}}$ with $\mu_m>0$ is

$$\begin{aligned}\frac{\Delta z_i}{c\,\Delta t}&(\psi_{i,m,g}^{\mathrm{L}}-\psi_{i,m,g}^{\mathrm{L},n-1/2})\\&+\mu_m[\psi_{i,m,g}^{\mathrm{L}}+\psi_{i,m,g}^{\mathrm{R}}-2\psi_{i-1,m,g}^{\mathrm{R}}]+\hat{\sigma}_{t,g}\,\Delta z_i\psi_{i,m,g}^{\mathrm{L}}\\&=\frac{1}{4\pi}\sigma_{s,i,g}\,\Delta z_i\phi_{i,g}^{\mathrm{L}}+\frac{1}{4\pi}\nu_i^{\mathrm{L}}\chi_{i,g}^{\mathrm{L}}\sum_{k=1}^{G}\sigma_{a,i,k}\,\Delta z_i\phi_{i,k}^{\mathrm{L}}\\&\quad+q_{i,g}^{\mathrm{L}}\,\Delta z_i+\frac{\Delta z_i}{c\,\Delta t}\,\psi_{i,m,g}^{\mathrm{L},n-1/2},\end{aligned}\quad(133)$$

where

$$\begin{aligned}\nu_i^{\mathrm{L/R}}=&\left[4\pi\sum_{g=1}^{G}\sigma_{a,i,g}\frac{\partial B_{i,g}^{\mathrm{L/R},n-1/2}}{\partial T}\right]\Bigg/\\&\times\left[\frac{C_v}{\Delta t}+4\pi\sum_{g=1}^{G}\sigma_{a,i,g}\frac{\partial B_{i,g}^{\mathrm{L/R},n-1/2}}{\partial T}\right],\end{aligned}\quad(134)$$

$$\chi_{i,g}^{\mathrm{L/R}}=\left[\sigma_{a,i,g}\frac{\partial B_{i,g}^{\mathrm{L/R},n-1/2}}{\partial T}\right]\Bigg/\left[\sum_{k=1}^{G}\sigma_{a,i,k}\frac{\partial B_{i,k}^{\mathrm{L/R},n-1/2}}{\partial T}\right],\quad(135)$$

$$\begin{aligned}q_{i,g}^{\mathrm{L/R}}=&\sigma_{a,i,g}B_{i,g}^{\mathrm{L/R},n-1/2}\\&+\frac{1}{4\pi}\nu_i^{\mathrm{L/R}}\chi_{i,g}^{\mathrm{L/R}}\left[Q_i^{\mathrm{L/R}}-4\pi\sum_{k=1}^{G}\sigma_{a,i,k}\frac{\partial B_{i,k}^{\mathrm{L/R},n-1/2}}{\partial T}\right].\end{aligned}\quad(136)$$

The linearized lumped equation for $\psi^{\mathrm{R}}_{i,m,g}$ with $\mu_m > 0$ is

$$\frac{\Delta z_i}{c\,\Delta t}(\psi^{\mathrm{R}}_{i,m,g} - \psi^{\mathrm{R},n-1/2}_{i,m,g}) + \mu_m[\psi^{\mathrm{R}}_{i,m,g} - \psi^{\mathrm{L}}_{i,m,g}] + \sigma_{t,g}\,\Delta z_i \psi^{\mathrm{R}}_{i,m,g} = \frac{1}{4\pi}\,\sigma_{s,i,g}\,\Delta z_i \phi^{\mathrm{R}}_{i,g} + \frac{1}{4\pi}\,\nu^{\mathrm{R}}_i \chi^{\mathrm{R}}_{i,g} \sum_{k=1}^{G} \sigma_{a,i,k}\,\Delta z_i \phi^{\mathrm{R}}_{i,k} + q^{\mathrm{R}}_{i,g}\,\Delta z_i. \tag{137}$$

The linearized lumped equation for $\mathrm{c}^{\mathrm{L}}_{i,m,g}$ with $\mu_m < 0$ is

$$\frac{\Delta z_i}{c\,\Delta t}(\psi^{\mathrm{L}}_{i,m,g} - \psi^{\mathrm{L},n-1/2}_{i,m,g}) + \mu_m[\psi^{\mathrm{R}}_{i,m,g} - \psi^{\mathrm{L}}_{i,m,g}] + \sigma_{t,g}\,\Delta z_i \psi^{\mathrm{L}}_{i,m,g} = \frac{1}{4\pi}\,\sigma_{s,i,g}\,\Delta z_i \phi^{\mathrm{L}}_{i,g} + \frac{1}{4\pi}\,\nu^{\mathrm{L}}_i \chi^{\mathrm{L}}_{i,g} \sum_{k=1}^{G} \sigma_{a,i,k}\,\Delta z_i \phi^{\mathrm{L}}_{i,k} + q^{\mathrm{L}}_{i,g}\,\Delta z_i. \tag{138}$$

The linearized lumped equation for $\mathrm{c}^{\mathrm{R}}_{i,m,g}$ with $\mu_m < 0$ is

$$\frac{\Delta z_i}{c\,\Delta t}(\psi^{\mathrm{R}}_{i,m,g} - \psi^{\mathrm{R},n-1/2}_{i,m,g}) + \mu_m[2\psi^{\mathrm{L}}_{i+1,m,g} - \psi^{\mathrm{L}}_{i,m,g} - \psi^{\mathrm{R}}_{i,m,g}] + \sigma_{t,g}\,\Delta z_i \psi^{\mathrm{R}}_{i,m,g} = \frac{1}{4\pi}\,\sigma_{s,i,g}\,\Delta z_i \phi^{\mathrm{R}}_{i,g} + \frac{1}{4\pi}\,\nu^{\mathrm{R}}_i \chi^{\mathrm{R}}_{i,g} \sum_{k=1}^{G} \sigma_{a,i,k}\,\Delta z_i \phi^{\mathrm{R}}_{i,k} + q^{\mathrm{R}}_{i,g}\,\Delta z_i. \tag{139}$$

The linearized lumped equation for T^{L}_i is

$$T^{\mathrm{L}}_i = \left[\sum_{g=1}^{G} \sigma_{a,i,g}\,(\phi^{\mathrm{L}}_{i,g} - 4\pi B^{\mathrm{L},n-1/2}_{i,g}) + Q^{\mathrm{L}}_i\right] \Bigg/ \left[\frac{C_{v,i}}{\Delta t} + 4\pi \sum_{g=1}^{G} \sigma_{a,i,g} \frac{\partial B^{\mathrm{L},n-1/2}_{i,g}}{\partial T}\right] + T^{\mathrm{L},n-1/2}_i. \tag{140}$$

The linearized lumped equation for T^{R}_i is

$$T^{\mathrm{R}}_i = \left[\sum_{g=1}^{G} \sigma_{a,i,g}\,(\phi^{\mathrm{R}}_{i,g} - 4\pi B^{\mathrm{R},n-1/2}_{i,g}) + Q^{\mathrm{R}}_i\right] \Bigg/ \left[\frac{C_{v,i}}{\Delta t} + 4\pi \sum_{g=1}^{G} \sigma_{a,i,g} \frac{\partial B^{\mathrm{R},n-1/2}_{i,g}}{\partial T}\right] + T^{\mathrm{R},n-1/2}_i. \tag{141}$$

Finally, we give the discrete diffusion equations used in our acceleration schemes. It is critical that the discretization of the diffusion equations be consistent with the discretization of the transport equation. Failure to ensure such consistency results in instabilities in problems with optically thick spatial cells and strong material-radiation coupling. We use a type of consistent linear-discontinuous diffusion differencing first suggested by Adams and Martin [17].

The equations for $\delta\phi^{\mathrm{L}}_{i,g}$ and $\delta\phi^{\mathrm{R}}_{i,g}$, respectively, are

$$2(\delta J_{i,g} - \delta J_{i-1/2,g}) + \sigma_{a,i,g}\,\Delta z_i\,\delta\phi^{\mathrm{L}}_{i,g} = \sigma_{s,i,g}\,\Delta z_i(\phi^{\mathrm{L},l+1/3}_{i,g} - \phi^{\mathrm{L},l}_{i,g}) \tag{142}$$

and

$$2(\delta J_{i+1/2,g} - \delta J_{i,g}) + \sigma_{a,i,g}\,\Delta z_i\,\delta\phi^{\mathrm{R}}_{i,g} = \sigma_{s,i,g}\,\Delta z_i(\phi^{\mathrm{R},l+1/3}_{i,g} - \phi^{\mathrm{R},l}_{i,g}), \tag{143}$$

where δJ denotes the flux error,

$$\delta J_{i+1/2,g} = \tfrac{1}{2}(\delta J_{i+1} + \delta J_{i,g}) + \tfrac{1}{4}(\delta\phi^{\mathrm{R}}_{i,g} - \delta\phi^{\mathrm{L}}_{i+1,g}), \tag{144}$$

$$\delta J_{i,g} = -\frac{\hat{D}_{i,g}}{\Delta z_i}(\delta\phi^{\mathrm{R}}_{i,g} - \delta\phi^{\mathrm{L}}_{i,g}). \tag{145}$$

At the left boundary, Eq. (144) becomes

$$\delta J_{1/2,g} = \tfrac{1}{2}\,\delta J_1 - \tfrac{1}{4}\,\delta\phi^{\mathrm{L}}_{1,g} + R^{\mathrm{L},l+1/3}_{B,g,m}, \tag{146}$$

where $R^{\mathrm{L},l+1/3}_{B,g,m}$ denotes the left boundary residual at iteration step $l + \frac{1}{3}$. In general, a boundary residual is nonzero only if the angular intensity does not satisfy the prescribed boundary condition,

$$R^{\mathrm{L},l+1/3}_{B,g,m} = \sum_{\mu_m>0} \mu_m(\psi^{\mathrm{L},l+1/3}_{B,g,m} - f^{\mathrm{L}}_{B,g,m})w_m, \tag{147}$$

where $\psi^{\mathrm{L},l+1/3}_{B,g,m}$ is the incident intensity on the left boundary, and $f^{\mathrm{L}}_{B,g,m}$ is the prescribed incident intensity. For the vacuum case, $f^{\mathrm{L}}_{B,g,m} = 0$, and for the reflective case, $f^{\mathrm{L}}_{B,g,m} = \psi^{\mathrm{L},l+1/3}_{1,g,m'}$, where $\mu_{m'} = -\mu_m$. At the right boundary, Eq. (144) becomes

$$\delta J_{N+1/2,g} = \tfrac{1}{2}\,\delta J_N + \tfrac{1}{4}\,\delta\phi^{\mathrm{R}}_{N,g} + R^{\mathrm{R},l+1/3}_{B,g,m}, \tag{148}$$

where $R^{\mathrm{R},l+1/3}_{B,g,m}$ is the right boundary residual at iteration step $l + \frac{1}{3}$,

$$R^{\mathrm{R},l+1/3}_{B,g,m} = \sum_{\mu_m<0} \mu_m(\psi^{\mathrm{R},l+1/3}_{B,g,m} - f^{\mathrm{R}}_{B,g,m})w_m. \tag{149}$$

Note that the flux errors can be eliminated from Eqs. (142) and (143) via Eqs. (144) and (145). This yields a closed linear system of equations for the angle-integrated intensity errors, which we solve directly using Gaussian elimination with partial pivoting.

The equations for $\delta\Phi_i^{\mathrm{L}}$ and $\delta\Phi_i^{\mathrm{R}}$, respectively, are

$$2(\delta\mathscr{J}_i - \delta\mathscr{J}_{i-1/2}) + \langle\sigma\rangle_i \Delta z_i \,\delta\Phi_i^{\mathrm{L}} = \nu_i^{\mathrm{L}} \sum_{g=1}^{G} \sigma_{a,i,g} \Delta z_i (\phi_i^{\mathrm{L},l+2/3} - \phi_i^{\mathrm{L},l}) \tag{150}$$

and

$$2(\delta\mathscr{J}_{i+1/2} - \delta\mathscr{J}_{i,g}) + \langle\sigma\rangle_i \Delta z_i \,\delta\Phi_i^{\mathrm{R}} = \nu_i^{\mathrm{R}} \sum_{g=1}^{G} \sigma_{a,i,g} \Delta z_i (\phi_{i,g}^{\mathrm{R},l+2/3} - \phi_{i,g}^{\mathrm{R},l}), \tag{151}$$

where $\delta\mathscr{J}$ denotes the frequency-integrated flux error,

$$\delta\mathscr{J}_{i+1/2} = \tfrac{1}{2}(\delta\mathscr{J}_{i+1} + \delta\mathscr{J}_{i,g}) + \tfrac{1}{4}(\delta\Phi_i^{\mathrm{R}} - \delta\Phi_{i+1}^{\mathrm{L}}), \tag{152}$$

$$\delta\mathscr{J}_{i,g} = -\frac{\langle D\rangle_i}{\Delta z_i}(\delta\Phi_{i,g}^{\mathrm{R}} - \delta\Phi_i^{\mathrm{L}}). \tag{153}$$

At the left boundary, Eq. (152) becomes

$$\delta\mathscr{J}_{1/2} = \tfrac{1}{2}\,\delta\mathscr{J}_1 - \tfrac{1}{4}\,\delta\Phi_1^{\mathrm{L}} + R_{B,m}^{\mathrm{L},l+2/3}, \tag{154}$$

where $R_{B,m}^{\mathrm{L},l+2/3}$ denotes the left boundary residual at iteration step $l + \frac{2}{3}$,

$$R_{B,m}^{\mathrm{L},l+2/3} = \sum_{g=1}^{G} \sum_{\mu_m>0} \mu_m(\psi_{B,g,m}^{\mathrm{L},l+2/3} - f_{B,g,m}^{\mathrm{L}})w_m, \tag{155}$$

and where $\psi_{B,g,m}^{\mathrm{L},l+2/3}$ is the incident intensity on the left boundary at iteration step $l + \frac{2}{3}$ and $f_{B,g,m}^{\mathrm{L}}$ is the prescribed incident intensity. At the right boundary, Eq. (152) becomes

$$\delta\mathscr{J}_{N+1/2} = \tfrac{1}{2}\,\delta\mathscr{J}_N + \tfrac{1}{4}\,\delta\Phi_N^{\mathrm{R}} + R_{B,g,m}^{\mathrm{R},l+2/3}, \tag{156}$$

where $R_{B,g,m}^{\mathrm{R},l+2/3}$ is the right boundary residual at iteration step $l + \frac{2}{3}$,

$$R_{B,g,m}^{\mathrm{R},l+2/3} = \sum_{g=1}^{G} \sum_{\mu_m<0} \mu_m(\psi_{B,g,m}^{\mathrm{R},l+2/3} - f_{B,g,m}^{\mathrm{R}})w_m. \tag{157}$$

Note that the flux errors can be eliminated from Eqs. (150) and (151) via Eqs. (152) and (153). This yields a closed linear system of equations for the frequency-angle-integrated intensity errors, which is solved directly using Gaussian elimination with partial pivoting.

Our accelerated iteration scheme is rapidly convergent and appears to be unconditionally effective. Efficiency is demonstrated in the computational section.

7. COMPUTATIONAL RESULTS

In this section we perform calculations relating to the behavior of our scheme in the asymptotic equilibrium-diffusion limit with both resolved and unresolved boundary layers. We also perform calculations which demonstrate the effectiveness of our iterative convergence acceleration schemes: the diffusion-synthetic scheme and the linear multifrequency-grey scheme. All calculations were performed on a CRAY-YMP computer at Los Alamos National Laboratory.

The first set of calculations considers a problem nearly identical to the model half-space problem previously discussed. It consists of a 1D slab of aluminum with a thickness of 10 cm, radiation incident upon the left face, and a reflective boundary condition on the right face. Two calculations were performed for each of six incident intensity distributions: one with the boundary layer spatially resolved; one with the boundary layer spatially unresolved. Although the incident intensity distribution was varied, the total incoming radiation energy was always normalized to yield a surface temperature of 1.0 keV. The material temperature of the slab was initialized at 1.0 keV, and the radiation field was initialized to a 1.0 keV Planckian distribution. The incident angular distribution was either isotropic, nearly perpendicular (all radiation in the incident direction closest to $\mu = 1$), or nearly grazing (all radiation in the incident direction closest to $\mu = 0$). The frequency distribution was either Planckian or monoenergetic (all incident radiation in one group). In order to facilitate a proper comparison with the variational results of Pomraning, scattering was neglected in these calculations. The absorption coefficient tables were obtained for a 33-group set collapsed from the Los Alamos Astrophysical Library [18]. The group energy bounds (rather than frequency bounds) are given in Table I. When the incident intensity was monoenergetic, all of the radiation was put into group 14, which has an average energy of 1.165 keV. An S_{16} angular approximation with Gauss quadrature was used in all of the calculations. All calculations with an unresolved boundary layer were performed with 10 uniformly spaced cells, and all calculations with a resolved boundary layer were performed with 50 logarithmically spaced cells. The smallest cell in the logarithmic mesh was the leftmost cell, and the growth factor was 1.2 (i.e., each cell was 20% larger than the cell to its left). Each calculation was evolved in time until the steady-state solution was obtained. The quantities of interest that were calculated consisted of $T_{\infty,c}^{r}$, the computational value obtained for T_∞ with a resolved boundary layer; $T_{\infty,c}^{u}$, the computational value for T_∞ with an unresolved boundary layer; $T_{\infty,p}$, the value for T_∞ obtained using Pomraning's variational expression; and $T_{\infty,a}$, the value for T_∞ obtained from our discrete asymptotic analysis. These quantities are given for each of the six problems in Table II. Note that

TABLE I

33-Group Energy Structure

Group	Lower bound (keV)	Upper bound (keV)
1	1.00×10^{-5}	1.78×10^{-2}
2	1.78×10^{-2}	3.16×10^{-2}
3	3.16×10^{-2}	5.62×10^{-2}
4	5.62×10^{-2}	7.50×10^{-2}
5	7.50×10^{-2}	1.00×10^{-1}
6	1.00×10^{-1}	1.33×10^{-1}
7	1.33×10^{-1}	1.78×10^{-1}
8	1.78×10^{-1}	2.37×10^{-1}
9	2.37×10^{-1}	3.16×10^{-1}
10	3.16×10^{-1}	4.22×10^{-1}
11	4.22×10^{-1}	5.62×10^{-1}
12	5.62×10^{-1}	7.50×10^{-1}
13	7.50×10^{-1}	$1.00 \times 10^{+0}$
14	1.00	1.33
15	1.33	1.78
16	1.78	2.37
17	2.37	3.16
18	3.16	4.22
19	4.22	5.62
20	5.62	7.50
21	7.50	1.00×10^{-1}
22	1.00×10^{1}	1.33×10^{1}
23	1.33×10^{1}	1.78×10^{1}
24	1.78×10^{1}	2.37×10^{1}
25	2.37×10^{1}	3.16×10^{1}
26	3.16×10^{1}	4.22×10^{1}
27	4.22×10^{1}	5.62×10^{1}
28	5.62×10^{1}	7.50×10^{1}
29	7.50×10^{1}	1.00×10^{2}
30	1.00×10^{2}	1.33×10^{2}
31	1.33×10^{2}	1.78×10^{2}
32	1.78×10^{2}	2.37×10^{2}
33	2.37×10^{2}	3.00×10^{2}

values of both T and T^4 are given in Table II. This is appropriate since the radiation intensity is proportional to T^4.

Several trends in the data can be seen from Table II. First, $T^u_{\infty,c}$ is in fairly good agreement with $T^r_{\infty,c}$, indicating that our transport difference scheme is fairly accurate in the equilibrium diffusion limit, even with spatially unresolved boundary layers. As one might expect, the poorest agreement occurs for the incident intensity distribution that is the most nonequilibrium, the grazing/monoenergetic case. Second, the agreement between $T^u_{\infty,c}$ and $T_{\infty,a}$ is excellent, demonstrating the validity of our asymptotic analysis. Third, $T_{\infty,a}$ is in good agreement with $T_{\infty,p}$. This is expected since the expressions for these two quantities are quite similar. Surprisingly, $T_{\infty,a}$ seems to be more accurate than $T_{\infty,p}$ for the grazing-incidence cases. We suspect that this is simply fortuitous. Overall, it seems clear that the linear-discontinuous equations are not as accurate with unresolved boundary layers for the nonlinear case as they are for the linear case.

The second set of calculations performed relate to the efficiency of our acceleration schemes. Thompson scattering was included in all of the calculations. A total of three calculations were performed. Each corresponds to the model problem associated with the first set of calculations. The incident flux distribution was grazing in angle and mononergetic in frequency, and the magnitude of the intensity was normalized to achieve a surface temperature of 1.0 keV. The previously described spatial grid consisting of 50 logarithmically spaced cells was used in the calculations. The material temperature was initialized at 1.0 keV, and the radiation field was initialized to a 1.0 keV Planckian distribution. Each calculation was evolved in time for a total period of 10^{-8} s. The first calculation was performed with both diffusion-synthetic acceleration and multifrequency-grey acceleration. The second calculation was performed without convergence acceleration of any kind. The iterations in both the first and second calculations were carried out until the absorption rates satisfied a maximum pointwise relative change of less than 10^{-4}. The third calculation was carried out with both diffusion-synthetic acceleration and multifrequency-grey acceleration, but only one accelerated iteration was performed per time step. The temperature solutions from all three calculations are indistinguishable from one another when plotted on a linear

TABLE II

Results for Asymptotic Calculations

Incidence	Spectrum	$T^r_{\infty,c}$ (keV)	$T^{r\,4}_{\infty,c}$ (keV^4)	$T^u_{\infty,c}$ (keV)	$T^{u\,4}_{\infty,c}$ (keV^4)	$T_{\infty,p}$ (keV)	$T^4_{\infty,p}$ (keV^4)	$T_{\infty,a}$ (keV)	$T^4_{\infty,a}$ (keV^4)
Isotropic	Blackbody	1.00	1.00	1.00	1.00	1.00	1.00	1.00	1.00
Normal	Blackbody	1.05	1.22	1.04	1.17	1.04	1.17	1.04	1.17
Grazing	Blackbody	0.87	0.57	0.91	0.69	0.93	0.75	0.91	0.69
Isotropic	One-group	0.92	0.72	0.94	0.78	0.94	0.78	0.94	0.78
Normal	One-group	0.95	0.81	0.96	0.85	0.96	0.85	0.96	0.85
Grazing	One-group	0.84	0.50	0.90	0.66	0.92	0.72	0.90	0.66

TABLE III

Results for Time-Dependent Calculations

Calculation	CPU time (s)
1	795
2	125
3	61

scale varying from 0.85 keV to 1.35 keV. The CPU times for each calculation are given in Table III. It can be seen from Table III that the accelerated and converged calculation is more than six times faster than the unaccelerated calculation. Furthermore, the accelerated calculation with one iteration per time step is more than 13 times faster than the unaccelerated and converged calculation. In general we have found that one accelerated iteration per time step is adequate for realistic calculations. One of the reasons that this strategy works well is that energy is both locally and globally conserved with our algorithm after *each* accelerated iteration. The impact of this property is demonstrated for a closely related neutronics acceleration scheme in Ref. [15].

Although our discrete equations do not necessarily yield strictly positive solutions, we have found that any negative solutions tend to be relatively small. Negative intensities are not modified, but if negative temperatures are obtained, they are simply reset to a floor temperature. In principle, this can result in a nonphysical gain in material energy. However, it has been our experience that negative temperatures are so rare and so small that resetting them to the floor value has a negligible effect upon global energy conservation.

8. CONCLUSIONS AND FUTURE WORK

The linear-discontinuous scheme that we have developed appears to have excellent properties for radiative transfer calculations in stellar regimes. Well-behaved and fairly accurate solutions are obtained in the interior region even when boundary layers are unresolved by the spatial mesh. Our computational experience indicates that the scheme is quite robust, but not strictly positive. In those rare cases where negative temperatures are obtained, they can simply be reset to a floor temperature. The solution technique which we use is based upon source iteration in conjunction with diffusion-synthetic acceleration of the scattering source and linear multifrequency-grey acceleration of the emission source. We have found this technique to be sufficiently effective that only one accelerated iteration per time step is needed.

It is clear that our linear-discontinuous differencing scheme for radiative transfer is not as accurate with unresolved boundary layers as the traditional linear-discontinuous scheme for neutron transport. This is not surprising since nonlinear equations are generally more difficult to solve than linear equations.

Although we assumed that material properties are constant in each spatial cell, it is not necessary to do so. It seems possible that a variation in transport coefficients within each cell might improve the asymptotic behavior of our scheme near unresolved boundary layers. Adams and Nowak [19] have recently developed a differencing scheme that is very similar to our scheme, but which has transport coefficients at the left and right sides of each cell rather than a single set of transport coefficients within each cell. Their results indicate that two sets of transport coefficients per cell result in slightly better agreement with Pomraning's expression for T_∞.

Future work should include the generalization of our scheme to 1D spherical geometry and multidimensional geometries. The former task appears to be straightforward.

ACKNOWLEDGMENT

This work was performed under the auspices of the U.S. Department of Energy and the Defense Nuclear Agency.

REFERENCES

1. E. E. Lewis and W. F. Miller Jr., *Computational Methods of Neutron Transport* (Am. Nucl. Soc., Lagrange Park, IL, 1993).
2. E. W. Larsen, J. E. Morel, and W. F. Miller Jr., *J. Comput. Phys.* **69,** 283 (1987).
3. E. W. Larsen, *Nucl. Sci. Eng.* **112,** 336 (1992).
4. W. H. Reed, T. R. Hill, F. W. Brinkley, and K. D. Lathrop, LA-5428-MS, Los Alamos National Laboratory, 1973 (unpublished).
5. T. R. Hill, LA-5990-MS, Los Alamos National Laboratory, 1975 (unpublished).
6. M. Mordant, *Ann. Nucl. Energy* **8,** 657 (1981).
7. E. W. Larsen and P. Nelson, *SIAM J. Numer. Anal.* **19,** 334 (1982).
8. L. J. Lorence Jr., W. E. Nelson, and J. E. Morel, *IEEE Trans. Nucl. Sci.* **NS-32,** 4416 (1985).
9. E. W. Larsen and J. E. Morel, *J. Comput. Phys.* **83,** 212 (1989).
10. E. W. Larsen, G. C. Pomraning, and V. C. Badham, *J. Quant. Spectrosc. Radiat. Transfer* **29,** 285 (1983).
11. G. C. Pomraning, *J. Quant. Spectrosc. Radiat. Transfer* **36,** 69 (1986).
12. E. W. Larsen, *Transport Theory Statist. Phys.*, **13,** 107 (1984).
13. G. I. Marchuk and V. I. Lebedev, *Numerical Methods in the Theory of Neutron Transport* (Harwood Academic, New York, 1986).
14. J. E. Morel, E. W. Larsen, and M. K. Matzen, *J. Quant. Spectrosc. Radiat. Transfer* **34,** 243 (1985).
15. J. E. Morel and J. M. McGhee, *Nucl. Sci. Eng.* **116,** 73 (1994).
16. L. J. Lorence Jr., J. E. Morel, and E. W. Larsen, *Nucl. Sci. Eng.,* **101,** 341 (1989).
17. M. L. Adams and W. R. Martin, *Nucl. Sci. Eng.* **111,** 145 (1992).
18. W. F. Hubner, A. L. Merts, N. H. Magee, and M. F. Argo, Report LA-6760-M, Los Alamos, NM, 1977 (unpublished).
19. M. L. Adams and P. F. Nowak, submitted.